

Forecasts for Dark Energy Measurements with Future HI Surveys

Filipe B. Abdalla¹, Chris Blake², Steve Rawlings³

¹ *Department of Physics & Astronomy, University College London, Gower Street, London, WC1E 6BT, U.K.*

² *Centre for Astrophysics & Supercomputing, Swinburne University of Technology, Hawthorn, VIC 3122, Australia*

³ *Department of Astrophysics, University of Oxford, Denys Wilkinson Building, Keble Road, Oxford, OX1 3RH, U.K.*

21 October 2019

ABSTRACT

We use two independent methods to forecast the dark energy measurements achievable by combining future galaxy redshift surveys based on the radio HI emission line with Cosmic Microwave Background (CMB) data from the *Planck* satellite. In the first method we focus on the ‘standard ruler’ provided by the baryon acoustic oscillation (BAO) length scale. In the second method we utilize additional information encoded in the galaxy power spectrum including galaxy bias from velocity-space distortions and the growth of cosmic structure. We find that a radio synthesis array with about 10 per cent of the collecting area of the Square Kilometre Array (SKA), equipped with a wide ($10 - 100 \text{ deg}^2$) field-of-view, would have the capacity to perform a $20,000 \text{ deg}^2$ redshift survey to a maximum redshift $z_{\text{max}} \sim 0.8$ and thereby produce dark energy measurements that are competitive with surveys likely to be undertaken by optical telescopes around 2015. There would then be powerful arguments for adding collecting area to such a ‘Phase-1’ SKA because of the square-law scaling of survey speed with telescope sensitivity for HI surveys, compared to the linear scaling for optical redshift surveys. The full SKA telescope should, by performing a $20,000 \text{ deg}^2$ HI redshift survey to $z_{\text{max}} \sim 2$ around 2020, yield an accurate measurement of cosmological parameters independent of CMB datasets. Combining CMB (*Planck*) and galaxy power spectrum (SKA) measurements will drive errors in the dark energy equation-of-state parameter w well below the 1 per cent level. The major systematic uncertainty in these forecasts is the lack of direct information about the mass function of high-redshift HI-emitting galaxies. ‘Stacking experiments’ with SKA pathfinders will play an important role in resolving this uncertainty.

Key words: cosmology : radio surveys - galaxy power spectrum - baryonic oscillations - dark energy

1 INTRODUCTION

Over the past decade several different cosmological probes have collectively demonstrated that the Universe contains a large fraction of its energy density in clustered dark matter and unclustered dark energy. The analysis of the angular distribution of the Cosmic Microwave Background (CMB) anisotropies requires that the total energy density is close to that predicted in a spatially-flat Universe. This data, given a strong prior on the Hubble constant (Spergel et al. 2007) imposed by the Hubble Key Project (Freedman et al. 2001), yields evidence for unclustered dark energy. In a Universe that is close to spatially flat, observations of distant Type-Ia supernovae provide independent evidence for a dark energy component with a negative pressure driving an accelerated expansion (Riess et al. 2006). Furthermore, the anal-

ysis of the shape of the galaxy power spectrum at low redshift requires a matter density $\Omega_m \sim 0.25$ (e.g. Percival et al. 2007), and the corresponding measurement of baryon acoustic oscillations (BAOs) at $z = 0.35$ agrees with this picture (Percival et al. 2007). Other probes confirm this paradigm: a positive cross-correlation of the distribution of the photons of the CMB with the distribution of galaxies at low redshift indicates, via the Integrated Sachs-Wolfe (ISW) effect, that the growth of large-scale over-densities is consistent with the presence of dark energy with a negative pressure. The ISW effect has been detected at the $> 2.5\text{-}\sigma$ level by several groups (e.g. Boughn & Crittenden 2005; Cabré et al. 2006; Rassat et al. 2006; Giannantonio et al. 2006).

No model has yet been successful in fitting all of the above cosmological data without using a dark energy com-

ponent. This does not rule out a modified gravity model (e.g. Skordis et al. 2006; Mena et al. 2006) or more complex cosmological assumptions such as back-reaction from inhomogeneities (Räsänen 2004), although dark energy from back-reaction is disfavoured by other authors (Ishibashi & Wald 2006). However, the addition of a dark energy component is the model that is the best-supported phenomenologically to date, even though we do not have a clear understanding of its origin or its nature.

Although there is a wealth of information indicating the existence of a dark energy component in our Universe, the measurements of its properties, and specifically its equation of state $w = p/(\rho c^2)$ (where p and ρc^2 are the pressure and energy density of dark energy respectively), are currently poor. The simplest explanation for dark energy is Einstein's cosmological constant, parameterized by $w = -1$, although the observed magnitude of this vacuum energy poses a formidable difficulty for theory. Current measurements of the parameter w are at the 10% level (Spergel et al. 2007).

The discovery that $w \neq -1$ would yield vital information on the nature of dark energy. If w is a function of time (i.e. redshift) and space, it could potentially approximate to a constant close to -1 at late times, depending on its nature and evolution with redshift (Simpson & Bridle 2006). The dark energy would therefore behave as a cosmological constant at the present day. We need to measure both this equation-of-state parameter w and its evolution with time in order to prove or disprove whether dark energy is due to the presence of a cosmological constant.

There are several types of observation which could in principle achieve a measurement of w with per-cent level accuracy, including weak gravitational lensing, supernovae, and cluster number counts. Future radio (HI emission) redshift surveys might make significant contributions to this quest by measuring the large-scale distribution, and hence clustering power spectrum, of galaxies (Blake et al. 2004; Rawlings et al. 2004; Abdalla & Rawlings 2005; Zhang & Pen 2006; Chang et al. 2008). The characteristic length scale of 'wiggles' in the matter power spectrum due to BAOs provides a set of 'standard rulers' at any epoch (i.e. redshift) at which they can be detected. BAO tests are especially promising for measuring dark energy as they are believed to be relatively immune to systematic effects (Blake & Glazebrook 2003; Seo & Eisenstein 2003; Hu & Haiman 2003). BAO measurements have already been successfully extracted from the Sloan Digital Sky Survey (SDSS) dataset (Eisenstein et al. 2005; Percival et al. 2007) and, although the relatively small volume of the Universe probed by SDSS only permits a measurement of Ω_m rather than an accurate determination of w , the prospects look extremely promising.

Developing a strategy for performing redshift surveys in radio wavebands is very different from planning counterparts in optical light. We discuss in this paper the advantages and disadvantages of a radio survey compared to an optical survey. We also make a prediction of how much information can be obtained by measuring the full galaxy power spectrum, and compare this to an analysis retaining only the clean signature of the BAOs.

In Sec.2 we discuss some of the differences between optical and radio surveys of large-scale structure. In Sec.3 we detail how we simulate HI surveys, also referring the reader

to Abdalla & Rawlings (2005). In Sec.4 we present forecasts for measuring dark energy from several sizes of radio surveys that should, alongside CMB data from the *Planck* satellite¹, be attainable over the coming decade. In Sec.5 we use Monte Carlo Markov Chain (MCMC) techniques to estimate the quality of future galaxy power spectra; see also Abdalla & Rawlings (2007). In Sec.6 we comment on the mitigation of potential systematic errors in the analysis. We conclude our findings in Sec.7.

Unless otherwise stated we adopt a Λ CDM model with an extra parameter w , a constant equation-of-state of dark energy. Based on recent measurements of cosmological parameters (Komatsu et al. 2008; Dunkley et al. 2008) we adopt the following choice of parameters for our fiducial cosmological model: $\{\Omega_b, \Omega_c, w, h, n_s, \sigma_8, \tau\} = \{0.04, 0.26, -1.0, 0.72, 1.0, 0.9, 0.09\}$, where Ω_b and Ω_c are the present-day density of baryons and cold dark matter expressed as a fraction of the critical density, $h = H_0/(100 \text{ km s}^{-1} \text{ Mpc}^{-1})$ represents the Hubble Constant, n_s is the primordial spectral slope of the power spectrum that has an overall present-day normalization σ_8 and τ is the optical depth to the last-scattering surface at recombination. We consider only models that are spatially flat (i.e. $\Omega_\Lambda = 0.7$ in our fiducial cosmology) and we ignore the effects of neutrinos and other forms of hot dark matter (Abdalla & Rawlings 2007).

2 A CRITICAL COMPARISON OF OPTICAL AND RADIO REDSHIFT SURVEYS

Undertaking 'all-sky' galaxy redshift surveys in optical and radio wavebands gives rise to very different issues. Although astronomers will be striving to complete both types of survey over the coming decade, there is a natural competitive tension between the techniques that is discussed in this Section.

The optical spectra of galaxies are much wealthier in information than their radio spectra. Optical galaxy spectra exhibit absorption features, and many have strong emission lines such as Ly α , [OII] and H α , making redshift determination straightforward with sufficient signal-to-noise. The information is sufficiently rich that one can pre-select a particular redshift range or type of galaxy from the colours derived from a photometric imaging survey. The rest-frame equivalent widths of some emission lines can be very large for subsets of galaxies, e.g. the star-forming galaxies, so blind surveys are also plausible via 'slit-less' techniques. Care must be taken in both targeted and blind surveys to account for interlopers from emission-line mis-identifications.

In the radio part of the spectrum the information in a galaxy spectrum is much more limited. The radio continuum is relatively featureless allowing for only the very crudest photometric redshift techniques, e.g. by using correlations between redshift and radio spectral index (Cruz et al. 2007). There is only one strong line in the radio spectrum – the '21-cm line' arising from hyperfine splitting in the hydrogen atom (HI) – and it is trivial for radio telescopes to obtain the spectral dimension as part of an imaging survey. Recent technological breakthroughs allow this to be achieved over

¹ <http://www.rssd.esa.int/Planck/>

large frequency bandwidths. In principle, clean and blind redshift surveys are therefore straightforward, with the luminosity of the HI line providing a direct measure of the HI mass in an object. HI line surveys are hence similar to blind optical emission-line searches performed with Integral Field Units (IFUs) or slit-less spectroscopy.

Unfortunately the HI line is extraordinarily weak. Thus, at the time of writing, all of the most important surveys of large-scale structure have been undertaken with optical telescopes. The state-of-the-art method of performing these surveys is to use wide-field ($\sim \text{deg}^2$) multi-object spectrograph that, because of the multiplex advantage of obtaining spectra of 10^{2-3} objects per pointing, have been able to build up catalogues containing 10^{5-6} redshifts using 10^{3-4} separate telescope pointings. With spectroscopic exposures of the order of hours these programmes take 10^{2-3} clear dark observing nights and therefore many years to complete with a single telescope. Surveys such as the SDSS have now mapped out significant fractions ($\sim 1/4$) of the sky, but only at low redshifts ($z \lesssim 0.5$) where moderate-sized (4-m class) telescopes can measure absorption-line galaxy redshifts with relative ease.

There are good prospects of pushing such studies to moderately-higher redshifts ($z \lesssim 1$) with 4-m-class ground-based telescopes. One technique is to target highly-biased tracers such as Luminous Red Galaxies, which require a lower target density to suppress shot noise in the power spectrum. In this manner the Baryon Oscillation Spectroscopic Survey (BOSS)², an extension of the SDSS, will reach $z \sim 0.7$ over 25% of the sky by 2014. Another technique is to focus on objects that have strong emission lines such as [OII], so that redshifts can be measured to a greater depth without requiring a detection of the galaxy continuum light. In this manner the WiggleZ survey (Glazebrook et al. 2007) at the Anglo-Australian Telescope (AAT) is probing galaxies up to $z \sim 1$ over 2.5% of the sky by 2010. Both of these approaches require a method of isolating specific types of high-redshift galaxies, such as by using colour cuts and/or photometric redshifts.

Optical surveys can be performed to still higher redshifts using the greater light grasp of 8-m class ground-based optical telescopes and optimized observational strategies. The recent deployment on the 8-m Subaru Telescope of the FMOS near-IR multi-object spectrograph (Dalton et al. 2006) will enable large-scale projects at near-IR wavelengths, allowing redshift surveys based on absorption-line (i.e. 4000-Å break) systems at $z \gtrsim 1$ and emission-line (i.e. H α) redshifts up to $z \sim 2$. There are also plans for wide-field red-sensitive optical multi-object spectrographs such as the proposed Wide Field Multi-Object Spectrograph (WF-MOS); this instrument would possess > 1000 fibres and have sufficient sensitivity to push wide-field optical redshift surveys to $z \sim 4$.

In principle, instruments like FMOS and WFMOS could survey the entire sky for a selection of galaxies. However, such surveys would be very slow for three main reasons: (i) pre-selection of targets is hard, as existing imaging surveys are either small or too shallow to select targets; (ii) the field-of-view (*FOV*) of these spectrographs is of order one

square degree and exposures could take most of a clear dark night at $z \gtrsim 1.5$ (with the exception of line emitting galaxies); and (iii) surveys must share time with other astronomical programmes or instruments and are relatively limited in duration. In practice these future ground-based optical redshift surveys will probably be limited to $\lesssim 2000 \text{ deg}^2$ of sky. Similar limitations on sky area apply to the alternative ground-based optical technique of obtaining ‘blind’ redshifts of high-redshift Ly α emitters using multiple IFUs deployed in the focal plane, such as proposed by the HETDEX experiment (Hill et al. 2008).

The most plausible approach for performing an all-sky high-redshift spectroscopic galaxy survey in optical or infrared wavebands is to use a space-based platform, as suggested by several candidate proposals for the Joint Dark Energy Mission (JDEM)³ funded in the United States or the ‘Euclid’ mission (Refregier & the DUNE collaboration 2008; Cimatti & the SPACE collaboration 2008) funded in Europe. The extremely low sky background from space enables much faster surveys, and galaxy pre-selection can be avoided using slit-less techniques detecting high-redshift H α -emitting galaxies up to $z \sim 2$. JDEM could be launched by 2015 if funding continues.

Future radio telescopes provide an alternative route to constructing all-sky galaxy redshift surveys up to $z \sim 2$. Radio telescopes benefit from a rapid rate of increase of survey speed with collecting area. The characteristic observing time t_{map} needed to detect all the HI line-emitting galaxies above a fixed line-flux limit over a fixed sky area scales with sensitivity and *FOV* in accordance with

$$\frac{1}{t_{\text{map}}} \propto f^2 \text{FOV} \quad (1)$$

where f is the fractional sensitivity of the telescope, which we define relative to a full SKA ($f \propto A_{\text{eff}}/T_{\text{sys}}$, where A_{eff} is the effective collecting area and T_{sys} is the system temperature). The quadratic nature of Eq.1 implies a fundamentally different scaling to the corresponding ETENDUE figure used to characterize the survey speed of optical telescopes ($1/t_{\text{map}} \propto A_{\text{eff}} \text{FOV}$ in the case of optical redshift surveys). Future radio interferometers will possess collecting areas which are orders of magnitude higher than those in operation today, and the technology exists to produce a field-of-view $\text{FOV} \sim 100 \text{ deg}^2$, significantly larger than achievable by optical spectrographs, and limited only by computational power. The large frequency bandwidth of the radio telescope will simultaneously map out a significant redshift range; the maximum redshift attained is determined by the sensitivity of the radio telescope and the degree of concentration of interferometric baselines in the telescope core.

In summary, although radio wavebands offer very limited possibilities for filtering techniques to pinpoint distant galaxies similar to those commonly used in optical wavebands, the sheer survey volume that future radio interferometers can map suggests that radio telescopes have the potential to become very competitive facilities for producing cosmologically-interesting redshift surveys.

A significant uncertainty in modelling future radio surveys is that radio techniques have so far only yielded direct

² <http://cosmology.lbl.gov/BOSS/>

³ <http://jdem.gsfc.nasa.gov/>

detections of HI emission to $z \sim 0.2$ (Zwaan et al. 2001; Verheijen et al. 2007). Various simple models extrapolating the properties of HI galaxies to higher redshifts are considered by Abdalla & Rawlings (2005); we emphasize here the critical role which SKA pathfinder telescopes will play in reducing these uncertainties to the level needed to optimize the design of the final SKA. Pathfinders such as ASKAP⁴ and MeerKAT⁵ will achieve significant expansions in frequency range and field-of-view over existing systems with similar sensitivity (i.e. $A_{\text{eff}}/T_{\text{sys}}$). One can then envisage a set of ‘stacking experiments’ that can yield statistical measures of HI at much higher redshifts than the $z \sim 0.2$ objects currently under study. The $\sim 30 \text{ deg}^2$ FOV expected to be delivered by ASKAP will allow deep-field observations covering (in ~ 3 pointings) $\sim 10^4$ ‘WiggleZ’ star-forming galaxies up to $z \sim 1$. Stacking the values of radio flux density in channels corresponding to HI at the optical redshifts of these objects provides, in the absence of any systematic noise floor, an $\sqrt{10^4} \sim 100$ -fold increase in effective sensitivity that more than compensates for the factor ~ 10 diminution of line flux expected between similar HI-emitting galaxies at $z \sim 0.2$ and $z \sim 1$. The sensitivity to be delivered by MeerKAT over smaller ($\sim 1 \text{ deg}^2$) sky patches will probe the general population of $z \sim 1$ galaxies: FMOS Guaranteed Time Observations (Dalton et al. 2006) expect to measure, via stellar absorption features as well as H α emission, redshifts for $\sim 10^4$ galaxies per square degree. These can also be stacked to achieve high-redshift statistical detections of HI, provided that the noise in the radio datasets is suitably well-behaved.

3 SURVEY MODELLING

We review here our method of simulating the HI surveys assumed in Sec.4 and Sec.5.2. In large part we have followed the prescription of Abdalla & Rawlings (2005), which we now clarify in more detail (see also Zhang & Pen (2006)).

3.1 HI mass limit

The r.m.s. sensitivity for a dual-polarization radio receiver at system temperature T_{sys} for an integration of duration t on a telescope of effective collecting area A_{eff} is given by the usual radio telescope equation⁶:

$$S_{\text{rms}} = \frac{\sqrt{2} C k_B T_{\text{sys}}}{A_{\text{eff}} \sqrt{\Delta\nu t}} \sim \left(\frac{1.6 \mu\text{Jy}}{f} \right) \sqrt{\frac{1}{\Delta\nu/\text{MHz}}} \sqrt{\frac{1}{t/\text{hr}}} \quad (2)$$

where C is a constant of order unity (see Chapter 1 of Thompson et al. 2001), k_B is Boltzmann’s constant, $\Delta\nu$ is the frequency bandwidth, and $f = [A_{\text{eff}}/(10^6 \text{ m}^2)][T_{\text{sys}}/50 \text{ K}]^{-1}$. The value of f hence parameterizes the sensitivity of the radio telescope compared to the SKA.

In practice we used for our calculations the frequency-dependent telescopes sensitivity listed in Table 1.2 of

Taylor & Braun (1999) which we express in the following fitting formula:

$$S_{\text{rms}} = \frac{(1.790365 \nu^2 - 4.53125 \nu + 4.46666) \mu\text{Jy}}{f} \times \sqrt{\frac{30 \text{ km/s}}{\Delta V}} \sqrt{\frac{4 \text{ hr}}{t}} \quad (3)$$

where ν is the frequency of the redshifted HI line. The first term in Eq.3 is equivalent to a dual-polarization r.m.s. sensitivity in a velocity channel of width $\Delta V = 30 \text{ km s}^{-1}$ in a $t = 4 \text{ hr}$ exposure. The underlying assumptions are that the scaling of S_{rms} with telescope sensitivity f is independent of frequency, and $C = \sqrt{2}$, which makes the optimistic assumption that all statistically-independent signal samples can be successfully averaged over a given exposure time. The assumption that f is independent of frequency implies that the increasing contribution of sky temperature to T_{sys} at lower frequencies is compensated for by an increase in A_{eff} with decreasing frequency. Given that the brightness temperature of the Galactic foreground emission scales roughly as $T_{\text{Gal}} \sim 20(\nu/408 \text{ MHz})^{-2.7} \text{ K}$, in practice this will become increasingly difficult to realize below $\sim 300 \text{ MHz}$ (HI at $z \sim 3.7$) once the rapidly rising sky temperature begins to dominate the system temperature.

The flux detection limit S_{lim} for galaxies is defined by the threshold parameter

$$n_\sigma = S_{\text{lim}}/S_{\text{rms}}. \quad (4)$$

We allow for a certain fraction of flux to be ‘resolved out’ using a model for the source sizes and the interferometric baseline distribution. The proper physical size of the sources is modelled as $R(z) = R_0/(1+z)^2$ following the discussion in AR05, where $R_0 = 15 \text{ kpc}$. The fraction of flux detected from a source at redshift z (see also Fig.2 of AR05) is then described as an integral over the distribution $f(B)$ of baselines B :

$$\text{Frac detected} = \int_{0 \text{ km}}^{10000 \text{ km}} f(B) \exp\left(-\frac{B^2}{2B_0(z)^2}\right) dB \quad (5)$$

where $B_0 = [\lambda x(z)]/[\pi R(z)]$ and $\lambda = 0.21 \text{ m}$, $x(z)$ is the co-moving radial distance to redshift z , and the baseline distribution $f(B)$ is given by

$$f(B) = \sum_i a_i \sqrt{\frac{2}{\pi}} \frac{1}{B_i} \exp\left(-\frac{B^2}{2B_i^2}\right) \quad (6)$$

where we use a sum of four different baseline components $i = 1$ to $i = 4$ where $B_1 = 0.5 \text{ km}$, $B_2 = 3 \text{ km}$, $B_3 = 150 \text{ km}$ and $B_4 = 2600 \text{ km}$ (this latter corresponding to 0.02 arc-sec resolution for wavelength $\lambda = 0.21 \text{ m}$). The coefficients a_i satisfy $\sum_{i=1}^4 a_i = 1$ (such that $\int f(B) dB = 1$) and were taken as $a_1 = 0.2242$, $a_2 = 0.2746$, $a_3 = 0.2506$, $a_4 = 0.2506$. This is a composite array and each a_i component of the array is distributed in a ‘scale-free’ configuration, as used in AR05. We note that the costs of data transport increase dramatically for the longest baselines of a radio interferometer and thus the final realization of the SKA is likely to be more centrally concentrated than we have assumed, meaning that we are being conservative in our assumed ability of the SKA to detect HI in galaxies.

The width of the HI emission line determines the relevant frequency bandwidth $\Delta\nu$ in Eq.2 and is related to a

⁴ <http://askap.pbwiki.com/>

⁵ <http://www.ska.ac.za/>

⁶ We note that the numerator of Eq.2 of Abdalla & Rawlings (2005) should read 100 mJy not 100 nJy.

line-of-sight velocity width $V(z)$ at redshift z :

$$\Delta\nu = \left(\frac{\nu_0}{1+z} \right) \frac{V(z)}{c}, \quad (7)$$

where $\nu_0 = 1.4204$ GHz is the rest-frame frequency of the HI line, c is the speed of light and $V(z)$ is measured in the rest-frame of the galaxy. We follow AR05 in assuming a scaling with redshift for the typical rest-frame velocity width of the line $V(z) = V_0/\sqrt{1+z}$, where $V_0 = 300 \text{ km s}^{-1}$, and ignore the effects of inclination.

The luminosity of HI photons from a gas cloud of mass M_{HI} can be derived using atomic physics (see, e.g., Sec.2.2 of AR05). Assuming a flat profile for the emission line with frequency, we obtain the following equation linking M_{HI} with the observed flux density S_ν :

$$M_{\text{HI}} = \frac{16\pi}{3} \frac{m_H}{A_{12}hc} x(z)^2 S_\nu V(z) (1+z) \quad (8)$$

or in usual units:

$$M_{\text{HI}} = 0.235 M_\odot (x/\text{Mpc})^2 (S_\nu/\mu\text{Jy}) (V/\text{kms}^{-1}) (1+z) \quad (9)$$

where m_H is the atomic mass of hydrogen, A_{12} is the Einstein coefficient for the transition, h is Planck's constant, and $x(z)$ is the co-moving distance to redshift z .

3.2 HI mass function modelling

We assume that the HI mass function at all redshifts is described by a Schechter function for the number density of galaxies dn in a mass range dM :

$$\frac{dn}{dM} dM = \phi^* \left(\frac{M}{M^*} \right)^\alpha \exp \left[- \left(\frac{M}{M^*} \right) \right] \frac{dM}{M^*} \quad (10)$$

parameterized by a low-mass slope α , a characteristic mass M^* and a normalization ϕ^* . This function has only been measured in the local Universe. The HIPASS survey reported the results: $\alpha = -1.3$, $M^* = 3.47 h^{-2} 10^9 M_\odot$, $\phi^* = 0.0204 h^3 \text{ Mpc}^{-3}$ (Zwaan et al. 2003)⁷. Throughout this study we assume $\alpha = -1.3$ at all redshifts. Our survey mass limit typically lies above M^* , thus our results are largely insensitive to the value of α . The HI mass function model must specify the redshift-evolution of $M^*(z)$ and $\phi^*(z)$.

By integrating the mass function we can deduce the overall mass density of neutral hydrogen at a given redshift:

$$\rho_{\text{HI}}(z) = \phi^*(z) M^*(z) \Gamma(\alpha + 2), \quad (11)$$

where Γ denotes the Gamma function. We used the HIPASS survey mass function measurements to fix the value of $\rho_{\text{HI}}(0)$. In order to model the evolution of ρ_{HI} with redshift, we followed AR05 and employed the measurements of the neutral gas density in damped-Ly α (DLA) systems as a function of redshift by Péroux et al. (2001). Specifically, we used the following functional form produced by AR05 by fitting to DLA data points, making a somewhat ad-hoc correction for selection effects in the damped-Ly α studies:

$$\Omega_{\text{HI}}(z) = N [1.813 - 1.473 (1+z)^{-2.31}] \quad (12)$$

⁷ We note that due to missing factors of h in a plotting routine, Fig.4 of Abdalla & Rawlings (2005) is incorrect, and it should be replaced by Fig.1 of this paper.

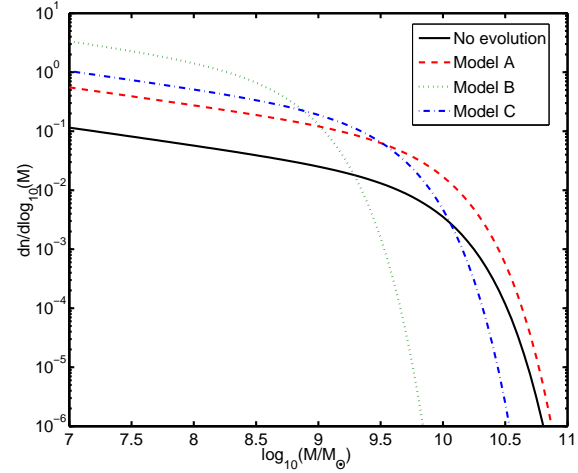


Figure 1. The HI mass function plotted at redshift $z = 2$ for a no-evolution model (black solid line), evolutionary models A (red dashed line), B (green dotted line) and C (blue dot-dashed line). This is a new version of Fig.4 from AR05 which was incorrect due to missing factors of h in the plotting routine. The evolutionary models are described in Sec. 3.2.

where $\Omega_{\text{HI}}(z) = \rho_{\text{HI}}(z)/\rho_c(z=0)$ is the HI mass density relative to the critical density of the Universe ($\rho_c(z=0) = 2.7755 h^2 10^{11} M_\odot \text{ Mpc}^{-3}$). The normalization constant is fixed by the zero-redshift HIPASS results.

If we use Eq.12 to determine the redshift-variation of the normalization of the mass function, then the full evolution model may be specified by the behaviour of the break in the Schechter function, $M^*(z)$. AR05 consider four different possibilities that, subject to the observational uncertainties in HI evolution detailed in the caption to Fig.2, span the plausible range of behaviours. We summarize these here, referring the reader to AR05 for a more detailed discussion:

- **No-evolution model:** ϕ^* and M^* remain equal to the zero-redshift values measured by the HIPASS survey.
- **Model A:** ϕ^* scales with z using the DLA results (Eq.12) with $M^*(z) = M^*(0) = \text{assumed constant}$.
- **Model B:** ϕ^* scales with z using the DLA results. $M^*(z) = M^*(0) D(z)^3$, where $D(z)$ is the linear growth factor at redshift z normalized such that $D(0) = 1$.
- **Model C:** ϕ^* scales with z using the DLA results. The break in the mass function is additionally controlled by the cosmic star formation rate.

In model C the break in the mass function evolves as

$$\frac{M^*(z)}{M^*(0)} = \left(\frac{[\Omega_{\text{stars}}(0)/\Omega_{\text{HI}}(0)] + 2}{[\Omega_{\text{stars}}(z)/\Omega_{\text{HI}}(z)] + 2} \right) D(z)^3 \quad (13)$$

where the fractional density in stars $\Omega_{\text{stars}}(z) = \rho_{\text{stars}}(z)/\rho_c(z=0)$ is deduced using the fits to the cosmic star-formation history in Choudhury & Padmanabhan (2002) and there is an implicit assumption that $\Omega_{\text{HI}}(z) = \Omega_{\text{H}_2}(z)$. Specifically,

$$\Omega_{\text{stars}}(z) = \frac{1}{\rho_c(z=0)} \int_z^\infty \left[\frac{SFR(z')}{H(z')(1+z')} \right] dz' \quad (14)$$

where $H(z)$ is the Hubble parameter at redshift z and we

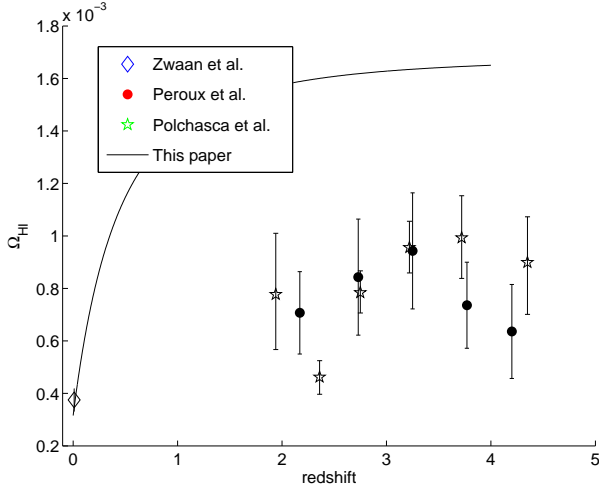


Figure 2. Measurements of the evolution of the HI mass density relative to the critical density of the Universe, $\Omega_{\text{HI}}(z)$, derived from HI emission studies (Zwaan et al. 2005) and studies of damped-Ly α absorption lines in distant quasars (Prochaska et al. 2005; Péroux et al. 2005). We have corrected all data to our fiducial cosmological model. The solid line shows the evolutionary behaviour assumed in this paper, we have assumed following AR. This line adopts the maximal correction (factor 2) inferred from radio-selected samples for dust biasing against the optical detection of HI-rich systems in absorption (Ellison et al. 2001). A recent study combining absorption-system results from optical- and radio-selected samples (Pontzen & Pettini 2008) suggests that the correction factor is unlikely to be much more than 1.3 subject to the caveat that a complete understanding of this factor requires more careful consideration of the effects of gravitational lensing, as well as dust, bias.

take

$$SFR(z) = \left[\frac{0.13}{1 + 6 \exp(-2.2z)} \right] \left[\frac{2}{2.5} \right] \left[\frac{x_{\text{fid}}(z)}{x(z)} \right] \quad (15)$$

where $x(z)$ is the co-moving distance to redshift z and $x_{\text{fid}}(z)$ is the value of $x(z)$ assuming a fiducial cosmology with $\Omega_{\text{m}} = 1$ to convert from the cosmology assumed by Choudhury & Padmanabhan (2002). The units of $SFR(z)$ in Eq.15 are $h^2 M_{\odot} \text{ yr}^{-1} \text{ Mpc}^{-3}$. There is an implicit assumption that $\Omega_{\text{HI}}(z) = \Omega_{\text{H}_2}(z)$; although $\Omega_{\text{HI}} \sim 4\Omega_{\text{H}_2}$ is more appropriate at low redshifts (Obreshkov & Rawlings 2008), model predictions of the cosmic evolution in the degree of molecularization in galaxies (Obreshkov et al., in prep) suggest that a rough equality becomes a reasonable assumption at $z \gtrsim 1$. Our default assumption will be evolution Model C, following the recommendation of AR05.

3.3 Survey parameters

We consider HI emission-line surveys defined by four parameters:

- The telescope sensitivity as a fraction of that achieved by the SKA (the parameter f in Eq.2).
- The survey detection threshold n_{σ} in Eq.4.
- The telescope field-of-view at the HI emission-line frequency at zero redshift, FOV .
- The assumed HI evolution model.

The scaling of the observed wavelength of the HI emission line with redshift can produce a corresponding scaling of the field-of-view FOV of the radio telescope, depending on the telescope design. We assume for now parabolic dishes with single-pixel feeds, such that $FOV \propto (1+z)^2$. This scaling may be used in a survey tiling scheme to produce an effective increase with redshift in the integration time t of the HI survey, and this is incorporated into our model following AR05.

We assume an overall survey duration equal to 1 yr covering approximately one hemisphere, 20,000 deg². We do not consider trade-offs between total survey area and redshift depth in this paper.

The bandwidth of the radio telescope may not be sufficient to cover the wavelength range of the HI emission line up to the maximum observable redshift z_{max} , necessitating repeat observations of each sky area. We use a parameter β to represent the ratio of the telescope bandwidth to the required frequency range of HI observations if we assume constant exposure time in each frequency block (in practice more distant redshift slices will require longer integrations and an ‘effective’ value of β will result). For example if $\beta \times FOV = 10 \text{ deg}^2$ then a 20,000 deg² survey requires 2000 pointings; if $\beta = 1$ each is of 4-hours duration, and this requires 1-year exposure time (adopting a 10 per cent overhead for calibration and other operational tasks). We note that, for a given survey duration and total solid angle, Eq.2 shows that the survey is identical if the combination $(\beta FOV f^2/n_{\sigma})$ remains unchanged. For example, halving the detection threshold n_{σ} is equivalent to doubling the field-of-view FOV or multiplying f by $\sqrt{2}$.

In subsequent calculations we adopt $f = 0.15$ as indicative of the sensitivity of an instrument representing ‘phase-I’ of the SKA (which may be available in 2015). Although it is anticipated that such an instrument will have ~ 10 per cent of the final collecting area of the SKA, it is likely for practical reasons to have a much larger fraction of its baselines within the compact core than is predicted by the baseline distribution function of Sec.3.1. Hence the sensitivity will be higher for fixed f as a greater fraction of baselines are useful for source detection.

3.4 Clustering of HI-emitting galaxies

We assume that the HI-emission galaxy power spectrum on large scales $P_{\text{HI}}(k)$ is related to the underlying linear dark matter power spectrum $P_{\text{lin}}(k)$ by a constant bias factor b , as is observed for all classes of galaxy on large scales:

$$P_{\text{HI}}(k) = b^2 P_{\text{lin}}(k) \quad (16)$$

HI-emitting galaxies are known to be one of the least biased tracers of mass over-densities (i.e. to possess one of the lowest values of b) owing to their avoidance of dense regions such as galaxy clusters. The clustering of the zero-redshift HIPASS survey has been measured by Basilakos et al. (2007) by fitting a power-law $\xi(r) = (r/r_0)^{-\gamma}$, with clustering length r_0 and slope γ . The results were $r_0 = 4.1 \pm 0.3 h^{-1} \text{ Mpc}$ (in redshift space) and $r_0 = 3.1 \pm 0.3 h^{-1} \text{ Mpc}$ (in real space), using the fixed canonical value $\gamma = 1.8$. This corresponds to a linear bias parameter $b = 0.63$.

No equivalent measurement exists at higher redshift,

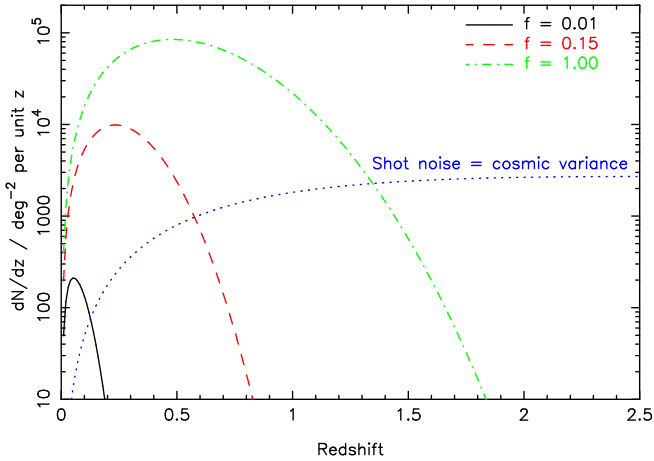


Figure 3. The dependence of the HI galaxy redshift distribution dN/dz on the fractional sensitivity f of the radio telescope (where $f = 1$ for the SKA), assuming 1 yr of observing and $\beta \times FOV = 10 \text{ deg}^2$. Other important assumptions are: (i) FOV scales with redshift as $(1+z)^2$; (ii) the baseline distribution and galaxy size assumptions of Sec.3.1 are adopted; (iii) HI evolution follows AR05 model C; (iv) only galaxies detected with a significance exceeding 10σ are considered.

but we note that many classes of galaxy evolve in their clustering such that $r_0(z) \approx \text{constant}$ where r_0 is measured in co-moving co-ordinates (e.g. Lahav et al. 2002). This forces a corresponding evolution in the linear bias $b \propto 1/D(z)$. Bias appears, however, to be a strong function of HI mass, in fact Basilakos et al. (2007) suggest that the more massive galaxies have a bias similar to optical galaxies, i.e. $b = 1$. For the purposes of this study and because of the lack of high-redshift measurements, we assume $b = 1$ independent of redshift; this is consistent with the clustering strength of objects near the break in the $z = 0$ HI mass function.

The clustering amplitude is significant in fixing the relative contribution of cosmic variance and shot noise to the error in a measurement of the power spectrum. These two sources of error are equal (at a given Fourier scale k) when the quantity $n \times P_{\text{HI}}(k) = 1$, where n is the galaxy comoving number density.

3.5 Redshift distributions

Figs.3 and 4 plot the HI galaxy redshift distribution dN/dz for various different survey parameters assuming detection threshold $n_\sigma = 10$. The source density corresponding to $n P_{\text{HI}}(k) = 1$ (for our assumed HI clustering properties) is also indicated, using the characteristic scale $k = 0.15 h \text{ Mpc}^{-1}$. The redshift at which dN/dz crosses this locus indicates the maximum redshift at which the error in the clustering measurements is dominated by cosmic variance rather than by shot noise.

In Fig.3 we assume $\beta FOV = 10 \text{ deg}^2$, $n_\sigma = 10$ and the preferred evolution model C, and plot dN/dz for fractional SKA areas $f = 0.01$, $f = 0.15$ and $f = 1$. In Fig.4 we fix $f = 1$ and plot dN/dz for $\beta FOV = 1, 10$ and 100 deg^2 . Note that an identical redshift distribution is produced if the survey parameters are changed such that the combination $(\beta FOV f^2/n_\sigma)$ is left invariant.

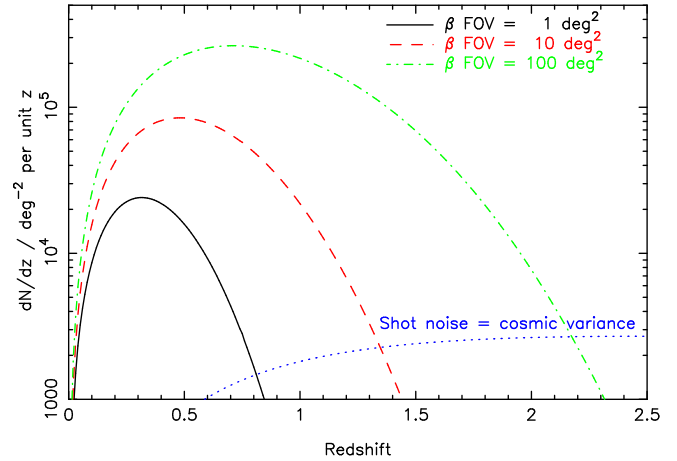


Figure 4. The dependence of the HI galaxy redshift distribution dN/dz on the quantity $\beta \times FOV$, assuming 1 yr of observing and a telescope sensitivity $f = 1$. See the caption to Fig.3 for other assumptions.

3.6 Effective survey volume

A useful ‘figure-of-merit’ for the accuracy with which a galaxy survey spanning a range of redshifts can measure the power spectrum at a given scale k is the *effective volume*. This is the cosmic volume weighted by a redshift-dependent shot-noise factor:

$$V_{\text{eff}}(k) = \int_0^\infty \left[\frac{n(z) P_{\text{HI}}(k, z)}{1 + n(z) P_{\text{HI}}(k, z)} \right]^2 \frac{dV}{dz} dz \quad (17)$$

In our assessment we take $k = 0.15 h \text{ Mpc}^{-1}$ as the relevant scale, because this defines the approximate extent of the linear regime at $z \approx 0.5$ and also characterizes the regime of interest for the baryon oscillations.

In Figs.5 and 6 we display the variation of the HI survey effective volume with the telescope sensitivity f over the range from $f = 0.01$ to $f = 1$. For comparison we also indicate the approximate volume that is likely to be probed by ground-based surveys in optical wavebands on a timescale of 2015. We base this benchmark – $V_{\text{eff}} = 5 h^{-3} \text{ Gpc}^3$ – on a projection of results from the Baryon Oscillation Spectroscopic Survey (BOSS) or the proposed Wide Field Multi-Object Spectrograph (WFMOs). This volume is equivalent to a survey of $10,000 \text{ deg}^2$ covering $z < 0.7$, or 2000 deg^2 spanning $0.5 < z < 1.5$ (if we neglect the shot noise factor in Eq.17). We note that assuming near-infra red spectroscopy, space-based surveys such as Euclid or JDEM would cover galaxies a redshift range of roughly $z < 2.0$ (Cimatti & the SPACE collaboration 2008), hence a similar volume achievable by a full SKA.

In Fig.5 we assume evolution model C and consider six different combinations of field-of-view and detection threshold. We note that the minimum sensitivity required by a radio telescope to equal the effective volume of our future optical survey benchmark (assuming $n_\sigma = 10$) are:

- $\beta FOV = 1 \text{ deg}^2 \rightarrow f = 0.4$
- $\beta FOV = 10 \text{ deg}^2 \rightarrow f = 0.13$
- $\beta FOV = 100 \text{ deg}^2 \rightarrow f = 0.04$

This is consistent with the quantity $FOV \times f^2$ characterizing the survey capability of radio telescopes.

In Fig.6 we assume $\beta FOV = 10 \text{ deg}^2$ and $n_\sigma = 10$ and display the dependence of the effective volume on the HI evolution model. The above conclusions regarding required collecting area are not strongly changed if a different evolution model is considered. In the most pessimistic case, an extra $\approx 50\%$ of sensitivity is required.

3.7 Maximum survey redshift

We used the criterion $n P_{\text{HI}}(k) = 1$ to estimate the maximum redshift z_{max} reachable in our model survey. Figs.7 and 8 display the dependence of this maximum redshift on the telescope collecting area in the same style as Figs.5 and 6. The HI radio surveys which match the performance of our benchmark future ground-based optical survey correspond to all-hemisphere surveys up to a maximum redshift $z \approx 0.6$ for an $f = 0.15$ radio array like the Phase-I SKA instrument. Surveys with a full SKA would access redshifts significantly beyond $z = 1$, perhaps reaching $z \sim 2$. Again, these conclusions do not depend strongly on the assumed HI evolution model.

4 SIMULATED DARK ENERGY MEASUREMENTS USING BARYON OSCILLATION FITTING

4.1 Survey power spectra

We divided each model HI survey into redshift slices of width $\Delta z = 0.2$ up to the maximum redshift z_{max} defined in Sec.3.7 (rounding up to the next multiple of Δz). For each redshift slice we modelled the error in the measurement of the galaxy power spectrum $P_{\text{HI}}(k)$ in each of a series of Fourier bins of width $\Delta k = 0.01 h \text{ Mpc}^{-1}$:

$$\delta P_{\text{HI}}(k, z) = \frac{1}{\sqrt{m}} \left[1 + \frac{1}{n(z) P_{\text{HI}}(k, z)} \right] \quad (18)$$

where $n(z)$ is the HI galaxy number density at redshift z , and m is the number of Fourier modes appearing in the bin of width Δk :

$$m = \frac{1}{2} \times \frac{V}{(2\pi)^3} \times 4\pi k^2 \Delta k \quad (19)$$

where V is the total survey volume. The power spectrum errors in each of the redshift slices are displayed in the panels of Fig.9 for four example surveys:

- **Parameter set 1:** $f = 1$, $\beta FOV = 10 \text{ deg}^2$, $n_\sigma = 10$.
- **Parameter set 2:** $f = 0.15$, $\beta FOV = 10 \text{ deg}^2$, $n_\sigma = 10$.
- **Parameter set 3:** $f = 0.01$, $\beta FOV = 10 \text{ deg}^2$, $n_\sigma = 10$.
- **Parameter set 4:** $f = 0.15$, $\beta FOV = 10 \text{ deg}^2$, $n_\sigma = 5$.

In each case the model power spectra and errors have been divided by a ‘reference’ power spectrum which possesses the same broadband shape and amplitude as the model power spectrum but has the BAOs erased, i.e. the

‘no-wiggles’ spectrum of Eisenstein & Hu (1998). Presenting the data in this manner illustrates the approximate significance with which the baryon oscillations are delineated by these surveys. The different redshift slices are offset vertically for clarity, and data points are plotted up to a maximum value $k = 0.2 h \text{ Mpc}^{-1}$, which is an estimate of the maximum extent of the linear regime at low redshifts, and which we then conservatively approximate as being independent of redshift. We note that an $f = 0.15$ SKA could produce a high-fidelity measurement of baryon oscillations in each of a series of redshift slices up to $z \approx 0.8$, if equipped with a field-of-view $\beta FOV \gtrsim 10 \text{ deg}^2$. A full SKA could return exquisite measurements of the galaxy power spectrum up to $z \approx 2$.

4.2 Fitting formula results

The BAOs in the galaxy power spectra act as a cosmological standard ruler which enables the cosmic distance and expansion rate at each survey redshift slice to be measured with high precision (Blake & Glazebrook 2003; Seo & Eisenstein 2003; Hu & Haiman 2003). Roughly speaking, oscillations in the tangential direction of the dataset can be used to accurately map the cosmic distance to each redshift slice. Radial oscillations return the Hubble parameter $H(z)$ at each slice.

Blake et al. (2006) devised fitting formulae which allow the survey parameters – central redshift z , volume V and galaxy number density n – to be converted into approximate accuracies of measurement of the tangential and radial baryon oscillation scales. These formulae are based on the procedure discussed by Blake & Glazebrook (2003) and Glazebrook & Blake (2005), which is designed to produce robust and conservative estimates of the standard ruler accuracies (see Seo & Eisenstein (2007) for a more recent fitting formula).

We used the fitting formulae of Blake et al. (2006) to determine the tangential and radial standard ruler accuracies in each of a series of redshift slices of width $\Delta z = 0.2$ for a variety of surveys varying collecting area f , detection threshold n_σ and field-of-view βFOV . We assume HI evolution model C. The results are plotted in Fig.10. The solid and dashed lines plot the tangential and radial accuracy, respectively, which are approximately equal to the accuracy with which the quantities $x(z)$ and $H(z)$ may be inferred in each redshift slice. This plot serves to emphasize the importance of a large field-of-view in extending the redshift range over which an HI survey can map cosmic distances. Future radio telescopes can produce per-cent-level measurements of $x(z)$ and $H(z)$ over a range of redshifts, provided that $\beta FOV f^2 \gtrsim 1$.

These measurements of cosmic distances and expansion rates may be readily converted into determinations of the parameters of the dark energy model. This is illustrated by Figs.11 and 12, corresponding to two different parameterizations of the dark energy equation of state: (1) $w(z) = w_{\text{cons}}$ (Fig.11) and (2) $w(z) = w_0 + w_a(1 - a)$, where $a = 1/(1+z)$ (Fig.12). We assume Gaussian priors on the other relevant cosmological parameters – Ω_m and h – parameterized as $\sigma(\Omega_m h^2) = 0.004$ and $\sigma(\Omega_m) = 0.01$. This is representative of the combination with measurements of the Cosmic Microwave Background anisotropies by the forthcoming *Planck* satellite. In detail, we assume that the baryon oscillations

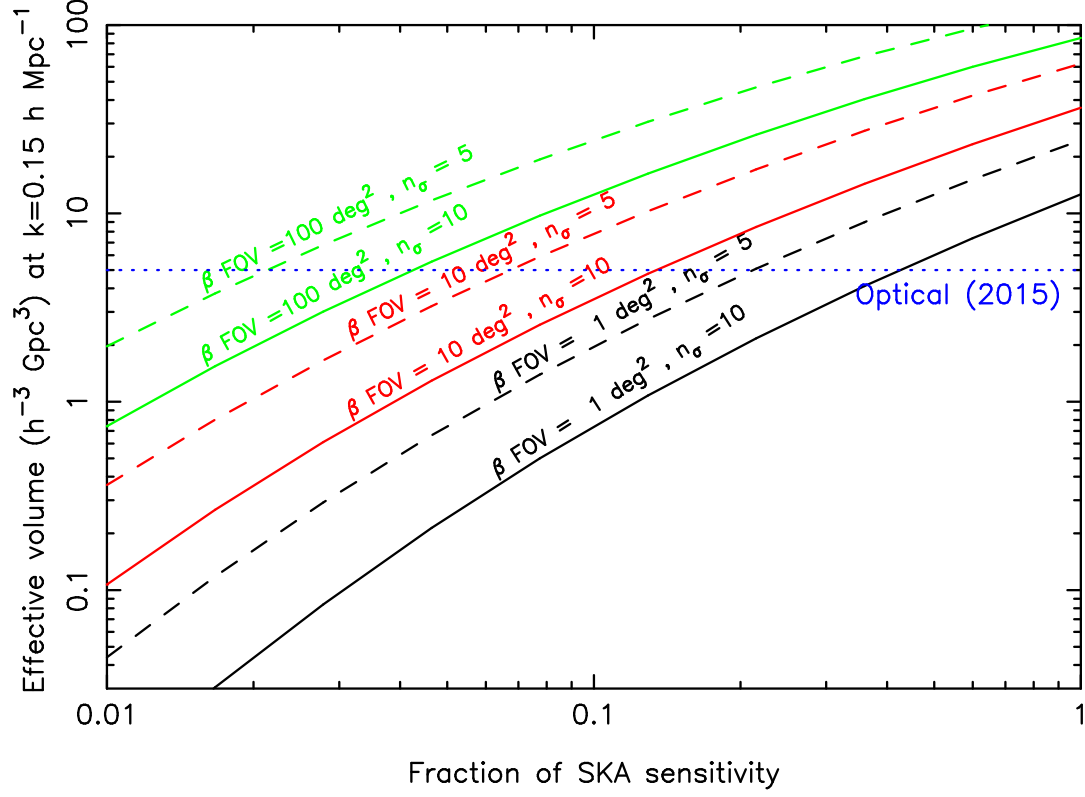


Figure 5. The dependence of the effective HI survey volume achieved in 1 yr of observing on the fraction of SKA sensitivity, for various different values of field-of-view ($\beta \times FOV$) and detection threshold n_σ . See the caption to Fig.3 for other assumptions. A rough benchmark is plotted for future ground-based redshift surveys in optical and near-infrared wavebands.

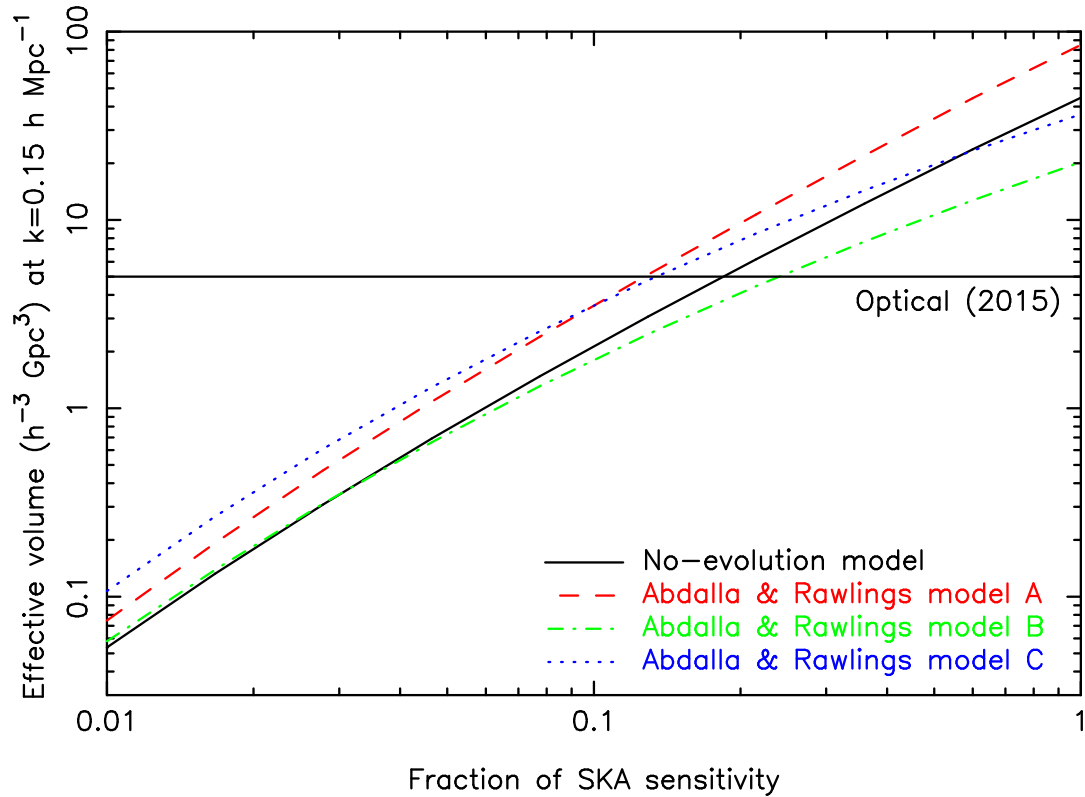


Figure 6. The dependence of the effective HI survey volume achieved in 1 yr of observing on the fraction of SKA sensitivity, for different HI evolution models. We assume $\beta \times FOV = 10 \text{ deg}^2$; see the caption to Fig.3 for other assumptions. A rough benchmark is plotted for future ground-based redshift surveys in optical and near-infrared wavebands.

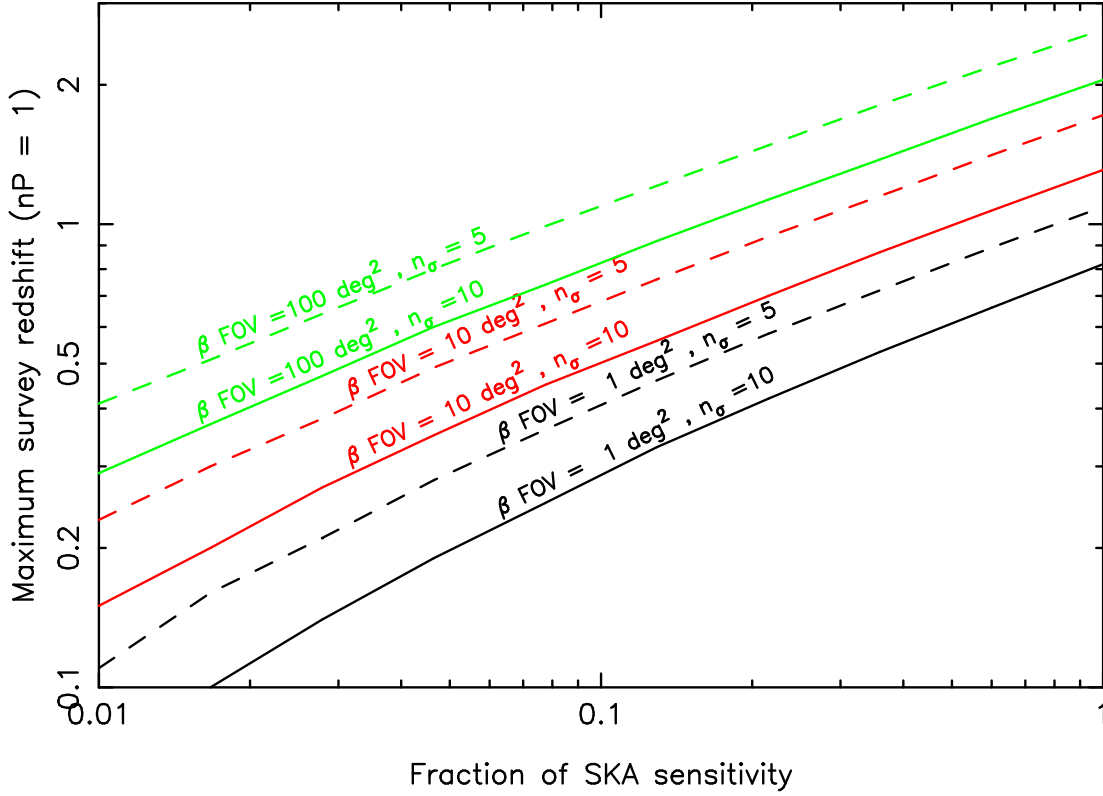


Figure 7. The dependence of the maximum HI survey redshift z_{max} achieved in 1 yr of observing on the value of $\beta \times \text{FOV}$ and detection threshold n_σ . See the caption to Fig.3 for other assumptions.

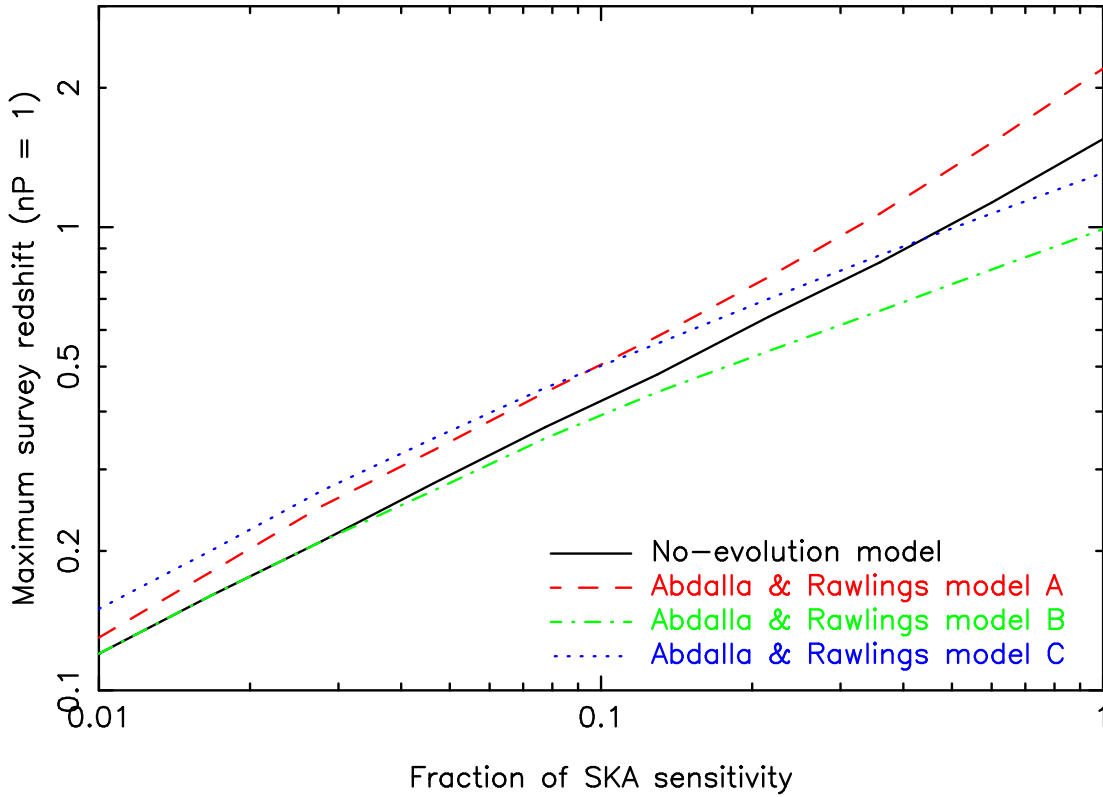


Figure 8. The dependence of the maximum HI survey redshift z_{max} achieved in 1 yr of observing on the fraction of SKA sensitivity, for different HI evolution models. A telescope with $\beta \times \text{FOV} = 10 \text{ deg}^2$ is assumed; see the caption to Fig.3 for other assumptions.

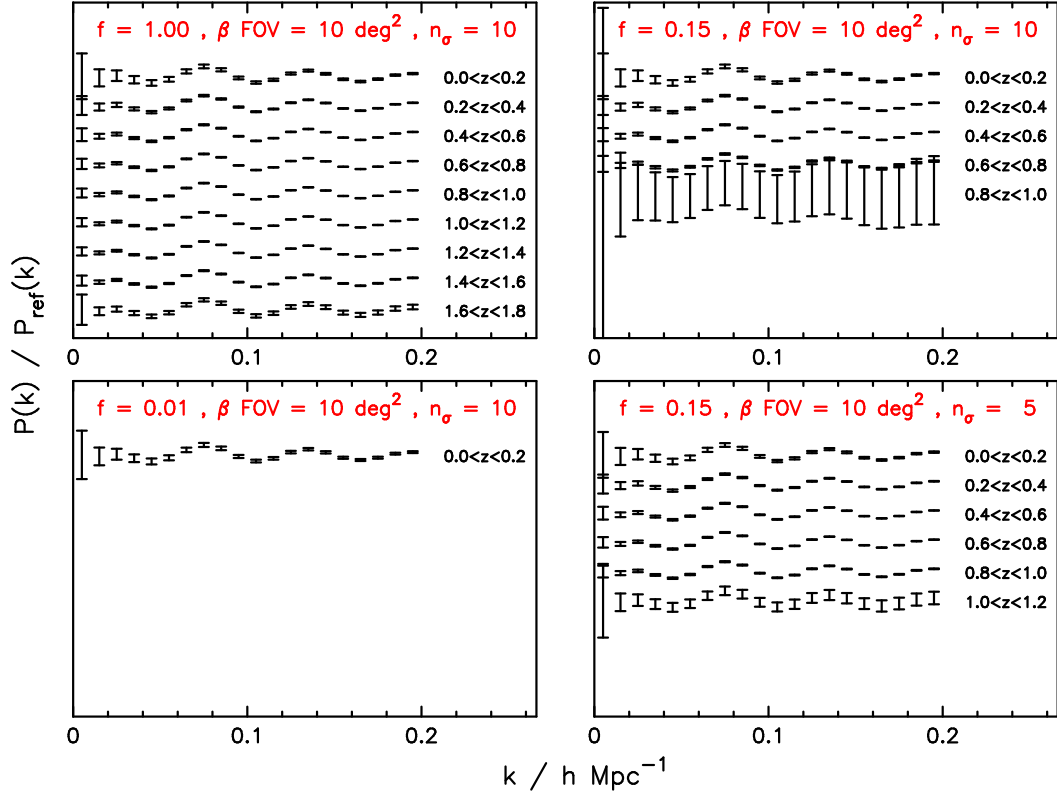


Figure 9. Power spectrum simulations for a series of redshift slices for four different HI survey parameter sets. The power spectra are divided by a smooth reference spectrum to emphasize the baryon acoustic oscillations. Power spectra for different redshift slices are offset vertically for clarity. Points are plotted up to a maximum value $k = 0.2 h \text{ Mpc}^{-1}$ which is an approximate estimate of the extent of the linear regime at low redshifts (Blake & Glazebrook 2003).

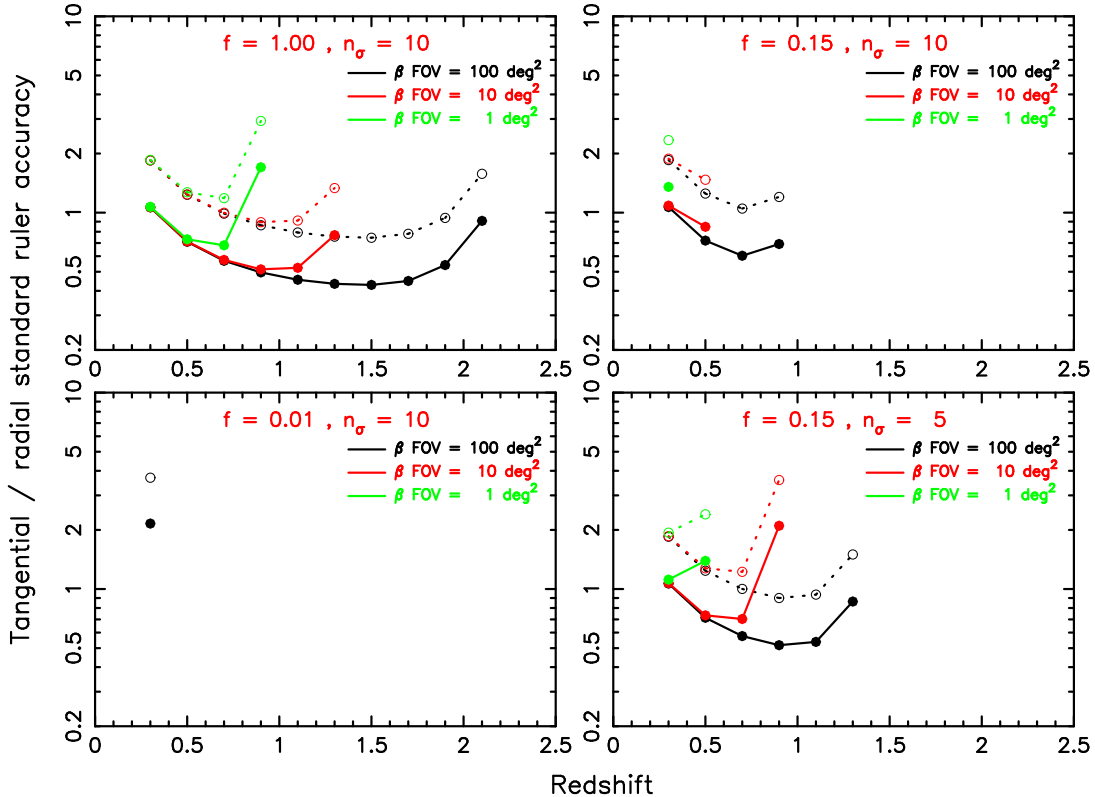


Figure 10. Simulated standard ruler accuracies in redshift slices of width $\Delta z = 0.2$ for a series of survey parameter sets defined by fractional SKA area f , threshold for source detection n_σ , and field-of-view $\beta \times \text{FOV}$. The solid lines indicate the simulated accuracy of measurement of the tangential acoustic scale; the dashed lines display the accuracy of the radial scale.

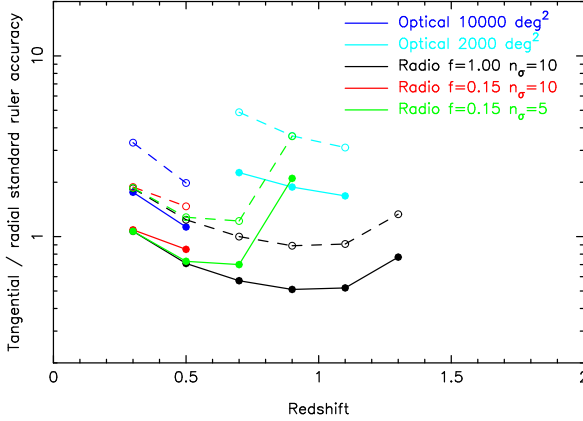


Figure 13. We plot here the accuracies in determining the angular diameter distance and the Hubble parameter from some model optical surveys, using the fitting formula described and we over-plot results for radio surveys. We have kept the binning in $dz=0.2$ redshift slices. The optical surveys we use are: $0.2 \leq z \leq 0.4$, 10000 deg^2 , $0.4 \leq z \leq 0.6$, 10000 deg^2 , $0.6 \leq z \leq 0.8$, 2000 deg^2 , $0.8 \leq z \leq 1.0$, 2000 deg^2 and $1.0 \leq z \leq 1.2$, 2000 deg^2 . $nP = 2$ for all surveys. $nP = 2$ refers to the product of the galaxy number density n in the redshift slice and the amplitude of the galaxy power spectrum P at $k=0.2$ (i.e. it is independent of galaxy bias) and ensures shot noise is significantly less than cosmic variance. The comparison radio surveys all have $\beta \text{FOV} = 10 \text{ deg}^2$, duration of one year, area of $20,000 \text{ deg}^2$. The solid lines (solid circles) are angular diameter distances accuracies and the dashed lines (open circles) are Hubble parameter accuracies.

provide a measure of $x(z)/s$ and $H(z)^{-1}/s$, where s is the sound horizon at recombination, and fold the uncertainties in Ω_m and h into the error in s .

An $f = 0.15$ SKA can produce a strong measurement of a constant dark energy equation of state ($\sigma(w_{\text{cons}}) \lesssim 0.1$) if $\beta \text{FOV} \gtrsim 10 \text{ deg}^2$. A full SKA produces $\sigma(w_{\text{cons}}) \approx 0.025$ for $\beta \text{FOV} = 10 \text{ deg}^2$. For an evolving equation of state parameterized by (w_0, w_a) , measurements at higher redshift assume increased importance. Here, an $f = 0.15$ SKA can produce a good measurement of the evolving term ($\sigma(w_a) \lesssim 1$) if $\beta \text{FOV} \gtrsim 50 \text{ deg}^2$ assuming $n_\sigma = 10$. A more aggressive threshold $n_\sigma = 5$ doubles the accuracy of the dark energy measurement in this case. A full SKA with $\beta \text{FOV} = 10 \text{ deg}^2$ allows parameter measurements of superb quality: $\sigma(w_0) \approx 0.05$ and $\sigma(w_a) \approx 0.2$. In Sec.5 we will compare these results with a full MCMC calculation.

We also plot in Fig.13 the accuracies in determining the angular diameter distance and the Hubble parameter from some model optical surveys using the fitting formula as we already described and over plotted onto results for radio surveys. This plot gives us an idea of the relative merit of optical surveys compared to radio surveys for cosmological parameter estimation. A binning of 0.2 in redshift was used and a number density for optical surveys was assumed to be $nP = 2$ (see Eqn.18), the product of the galaxy number density n in the redshift slice and the amplitude of the galaxy power spectrum P at $k = 0.2$ (i.e. it is independent of galaxy bias) – $nP = 2$ ensures shot noise is less than cosmic variance.

5 SIMULATED DARK ENERGY MEASUREMENTS USING A FULL POWER SPECTRUM ANALYSIS

We now perform simulations using the full power spectrum information to measure the dark energy model. The broad-band shape of the power spectrum depends mainly on the quantity $\Omega_m h$, and redshift-space distortions contain information on the large-scale bias of the galaxy population. Hence the power spectrum shape helps to break degeneracies in the cosmological model and sharpen our dark energy measurements. We refer the reader to Abdalla & Rawlings (2007) for a full description of our MCMC forecast method.

In this Section we assume a survey performed by an SKA with $\beta \times \text{FOV} = 10 \text{ deg}^2$. Therefore, a one-year survey corresponds to 4 hours integration time per pointing. There is a straight-forward trade-off between collecting area and integration time; when comparing different collecting areas we specify for reference the integration time required to achieve an equivalent depth with the full SKA ($f = 1$).

5.1 Effects of survey depth on parameter forecasts

We present in this subsection the effect that different collecting areas (or equivalently different integration times with a full SKA) have on the accuracy of cosmological parameter measurement for a $20,000 \text{ deg}^2$ survey. Initially we base the forecasts only on the SKA large-scale structure data and take a standard Λ CDM framework with an extra parameter w , a constant equation-of-state of dark energy. Our fiducial model is: $\{\Omega_b, \Omega_c, w, h, n_s, \sigma_8, \tau\} = \{0.04, 0.26, -1.0, 0.72, 1.0, 0.9, 0.09\}$. The fiducial bias of each redshift bin is $b = 1$, and we use three redshift bins in the analysis. We have tested that for a constant- w model there is negligible benefit from analyzing more redshift bins, although we note that this may not be the case for a more complex dark energy parameterization. We present in Table 1 our forecast errors in cosmological parameters recovered from the MCMC chains.

Using the large-scale structure data alone, our measurement error in w degrades sharply at a collecting area below $f \approx 0.35$ (or a 30-min exposure using the full SKA). This is because below this approximate threshold we are no longer able to break the degeneracies between the fitted parameters and we require additional data such as the CMB.

5.2 A combined experiment

We next forecast the cosmological parameter measurements achieved by combining the SKA large-scale structure survey with the CMB (*Planck*) dataset using the method of Abdalla & Rawlings (2007). We examine how an $f = 0.15$ SKA survey and an $f = 1$ SKA survey would benefit from the inclusion of CMB data. In order to combine the two datasets we add the log(likelihood) distributions assuming the datasets are uncorrelated.

We plot in Fig.15 the parameter measurements found for the combination of full SKA survey and CMB data. There are no significant degeneracies in any of the parameter pairs, as opposed to (for example) the $w - \sigma_8$ plane plotted in Fig.14 from the SKA survey alone (see also Fig.16). The CMB provides an accurate amplitude of fluctuations at the

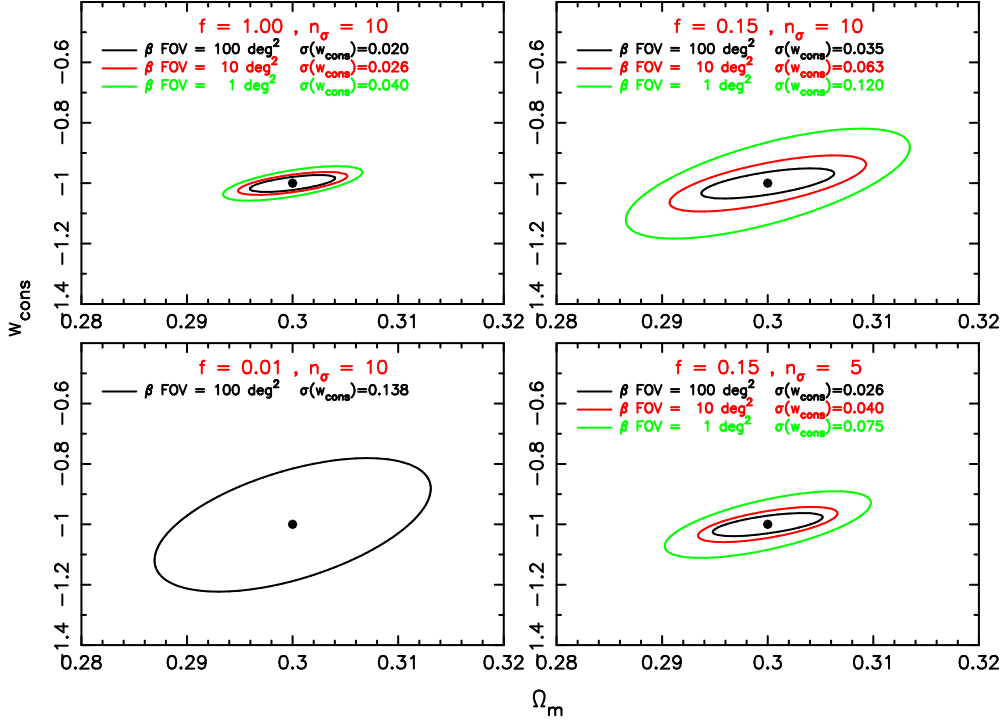


Figure 11. Simulated dark energy measurements of a constant equation-of-state $w(z) = w_{\text{cons}}$ for a series of surveys defined by fractional SKA sensitivity f , threshold for source detection n_σ , and field-of-view $\beta \times \text{FOV}$. $1-\sigma$ confidence ellipses are plotted in the parameter space of $(\Omega_m, w_{\text{cons}})$. Marginalized errors are shown for the parameter w_{cons} . The analysis uses the measurements of $x(z)$ and $H(z)$ using tangential and radial baryon oscillations, as displayed in Fig.10, together with Gaussian priors $\sigma(\Omega_m h^2) = 0.004$ and $\sigma(\Omega_m) = 0.01$, representative of combining with *Planck* satellite observations of the Cosmic Microwave Background.

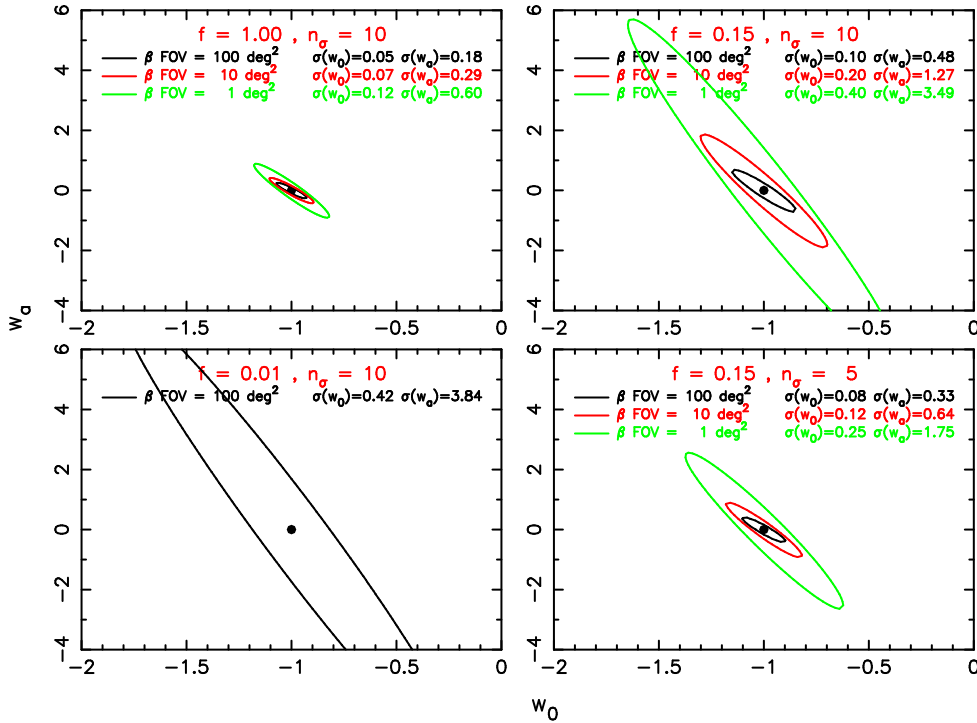


Figure 12. Simulated dark energy measurements of a redshift-dependent equation-of-state $w(z) = w_0 + w_a(1-a)$ for a series of surveys defined by fractional SKA sensitivity f , threshold for source detection n_σ , and field-of-view $\beta \times \text{FOV}$. $1-\sigma$ confidence ellipses are plotted in the parameter space of (w_0, w_a) . Marginalized errors are shown for w_0 and w_a . The analysis uses the measurements of $x(z)$ and $H(z)$ using tangential and radial baryon oscillations, as displayed in Fig.10, together with Gaussian priors $\sigma(\Omega_m h^2) = 0.004$ and $\sigma(\Omega_m) = 0.01$, representative of combining with *Planck* satellite observations of the Cosmic Microwave Background.

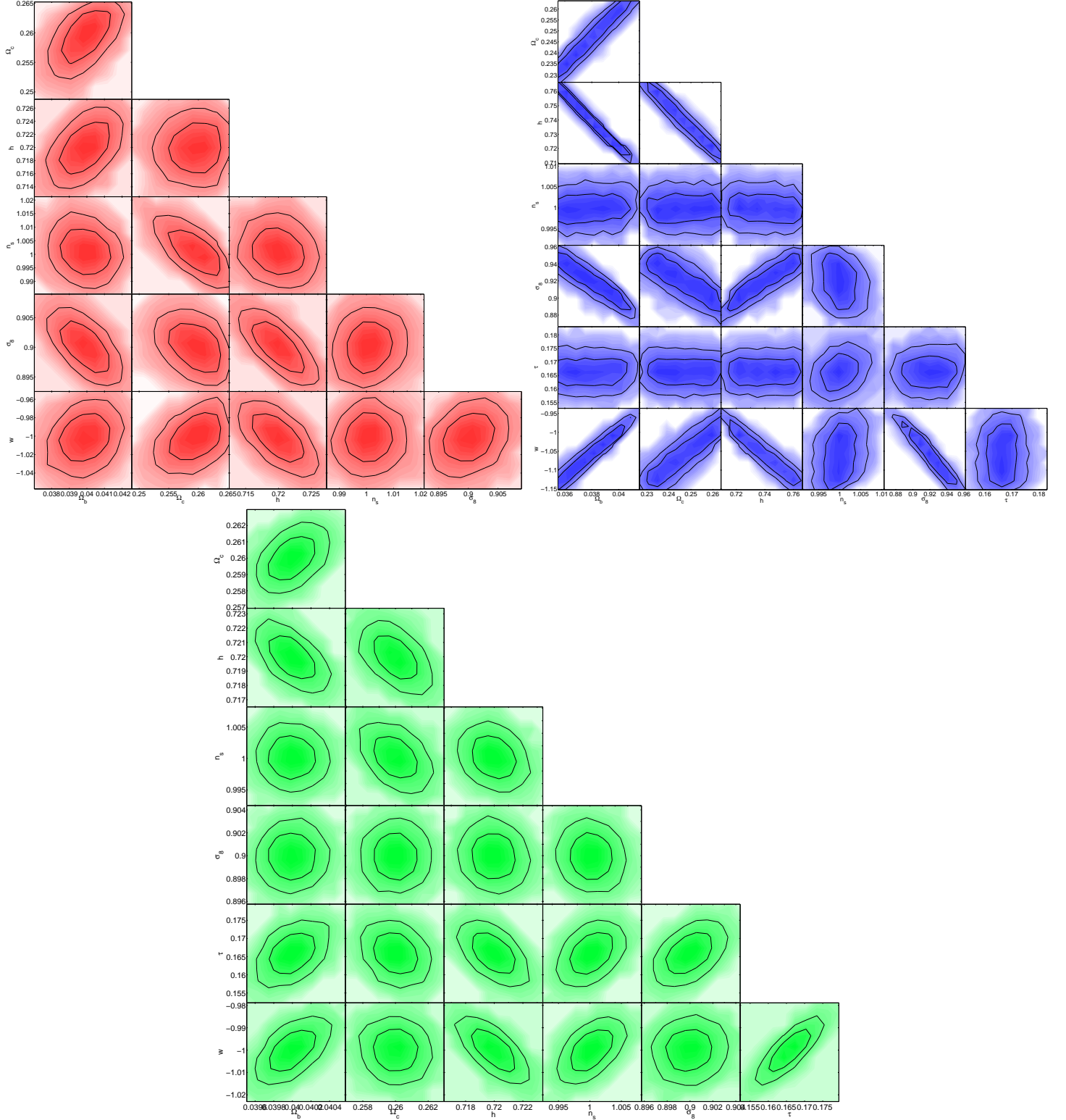


Figure 15. Analysis of the accuracy of a combination of future SKA (red), CMB (blue) and combined (green) experiments in measuring cosmological parameters. The contours represent one and two sigma confidence regions. The combination of SKA and CMB experiments will measure all current cosmological parameters to below the one per cent level, including the dark energy parameter w . The full SKA will produce a measurement of w with an accuracy close to 0.5%.

f	0.15	0.25	0.35	0.50	0.70	1	1.4	2
$f = 1$ SKA	0.1h	0.25h	0.5h	1h	2h	4h	8h	16h
z_{\max}	0.62	0.75	0.90	1.1	1.3	1.6	1.8	2.2
Ω_b	0.0040	0.0022	0.0014	0.0012	0.0011	0.00090	0.00080	0.00076
Ω_c	0.014	0.0078	0.0053	0.0042	0.0038	0.0031	0.0028	0.0021
w	0.32	0.081	0.036	0.026	0.022	0.017	0.015	0.013
n_s	0.051	0.023	0.012	0.0088	0.0073	0.0052	0.0050	0.0047
σ_8	0.061	0.022	0.0087	0.0054	0.0039	0.0028	0.0023	0.0020
h	0.043	0.013	0.0058	0.0042	0.0032	0.0025	0.0020	0.0020

Table 1. The forecast errors in cosmological parameters as a function of survey depth. The top row indicates the telescope sensitivity (for a 4-hr exposure); the second row lists the equivalent exposure time with a full SKA ($f = 1$). The third row details the approximate maximum redshift achieved, i.e. where $nP = 1$. For small integration times the errors in the dark energy equation-of-state w are large because the baryon oscillations are not measured accurately.

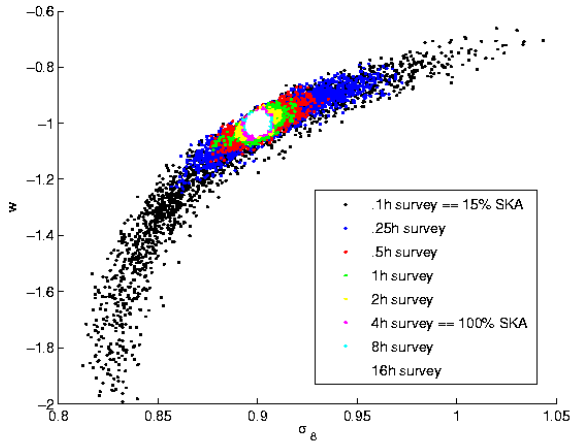


Figure 14. The posterior in the (σ_8, w) plane for full SKA surveys with different exposure times. The forecasts improve significantly from 6 mins exposure time (equivalent to 4 hrs with an $f = 0.15$ SKA) to 4 hrs exposure time with the full SKA. When we reach depths equivalent to a 1-hr exposure time with the full SKA, there are sufficient galaxies per unit volume and redshift to break the degeneracies and produce an accurate measurement of w .

last scattering surface, together with a measurement of the angular diameter distance to this surface, adding complementary information to the SKA dataset. In Table 2 we can see that there is a significant improvement in the parameter errors compared to those found in Table 1. The accuracy of measurement of the w parameter is below 1 per cent.

We also conclude from the simulations that most of the constraining power with regard to the parameter n_s originates from the CMB, and the LSS dataset adds little. This is because a high-resolution CMB experiment with a large multipole range (such as *Planck*) will measure CMB fluctuations across a large range in spatial scales. This picture could change if one were able to model non-linearities in the large-scale structure including a reliable biasing model at small scales. We surmise that the CMB data will be very useful in constraining some parameters, e.g. n_s , whilst LSS surveys will play an increasing role in the determination of other parameters, such as σ_8 and w (although the capacity

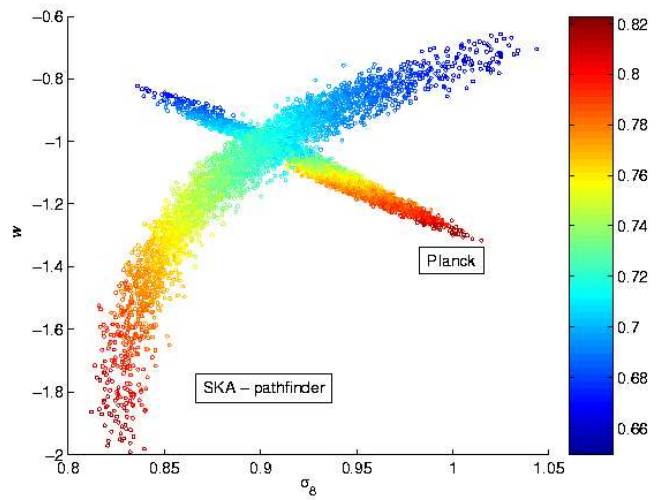


Figure 16. We illustrate one of the main degeneracies resolved when an HI survey dataset obtained with the $f = 0.15$ SKA is combined with a CMB (*Planck*) dataset. The degeneracy between σ_8 and w is broken and allows for a very good measurement of the dark energy parameter, even with a relatively shallow survey covering $20,000 \text{ deg}^2$. The samples are for independent MCMC chains for an $f = 0.15$ SKA and for *Planck*. They are colour-coded according to the value of h , as shown in the side-bar.

to measure σ_8 rests on a good model for the galaxy bias from redshift-space distortions).

We plot in Fig.16 the MCMC samples obtained for an $f = 0.15$ ‘phase I’ SKA combined with the future CMB data. In the absence of systematic errors this would yield errors in w of approximately 1 per cent. This forecast worsens by a factor of 2 if we assume that redshift-space distortions cannot be used to determine the galaxy bias factor, as discussed in the next Section.

5.3 Normalization factors

The results in Sec.5 rest on the assumption that redshift-space distortions can constrain the galaxy bias factor via large-scale bulk flows (Guzzo et al. 2008; Percival & White 2008). This information can also be provided by other

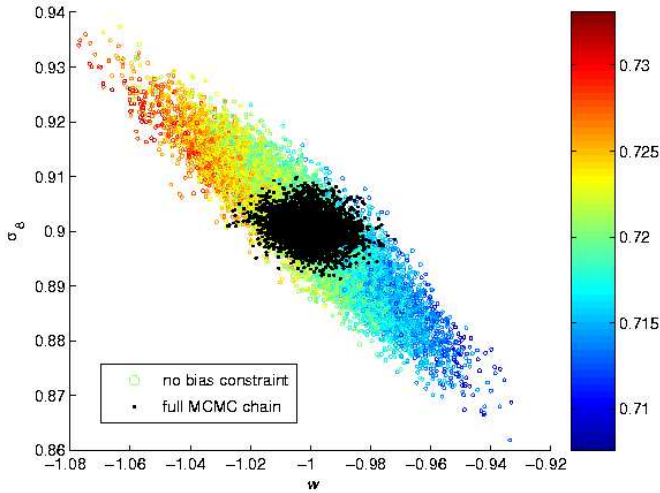


Figure 17. We demonstrate how the accuracy in measuring the value of the dark energy parameter w worsens if we cannot recover the galaxy bias information. In this case the distribution of MCMC chains changes from the black points to the coloured points, a degeneracy between σ_8 and w opens up, and the error in w degrades from 1% to 2.5%. The MCMC samples without bias information are colour-coded according to the value of h , as shown in the side-bar.

probes which we have not used here. Firstly, the analysis of the small-scale clustering in the framework of the galaxy halo model makes predictions for the large-scale bias and redshift-space effects. Secondly, higher-order clustering statistics yield information on the bias of galaxies (Verde et al. 2002). Reasonably accurate knowledge of the bias parameter(s) may be gleaned from these tools. The scale-dependence of bias may be tested by selecting galaxies with different clustering properties located in the same comoving volume (Cole et al. 2006), with the aim of decoupling the cosmological signal from the galaxy bias.

On the other hand, we should be cautious in making these assumptions, since it is not yet clear that the desired level of systematic error control can be achieved. In order to investigate the importance of the additional bias information we performed a simulation considering only the isotropized power spectrum obtained with an $f = 0.15$ SKA survey in conjunction with the *Planck* CMB data, thereby removing the information associated with the redshift-space distortions.

We find that the parameter which suffers most from the loss of the bias information is σ_8 , which is unsurprising given that it is directly related to the height of the power spectrum. In Fig.17 we plot results from simulations, both with and without bias measurements from redshift-space distortions. We find that without the bias information the accuracy of measurement of w is reduced from the one per cent level to roughly the two and a half per cent level, and there remains a residual σ_8 - w correlation.

Parameter	$f = 0.15$ SKA (1)	$f = 0.15$ SKA (2)	$f = 1$ SKA
Ω_b	0.00024	0.00044	0.00016
Ω_c	0.0016	0.0021	0.00086
w	0.010	0.022	0.0062
n_s	0.0024	0.0028	0.0021
σ_8	0.0026	0.010	0.0013
h	0.0019	0.0035	0.0010
τ	0.0042	0.0041	0.0036

Table 2. The forecast errors in cosmological parameters from simulations of an SKA HI survey plus CMB (*Planck*) data. The first column of results is for a ‘phase-I’ ($f = 0.15$) SKA and corresponds to a full analysis including the redshift-space distortions effect. The second column assumes that this information is unreliable and marginalizes over the large-scale anisotropic power. The final column compares these results to a full SKA survey including redshift-space distortions.

5.4 Comparison with BAO-only results

We can compare these MCMC calculations with our more approximate results presented in Sec.4. In the approximation of Sec.4 we only utilize the distance information encoded in the BAOs, not the full power spectrum shape. In addition we incorporate the CMB data only as ‘representative’ priors in the values of $\Omega_m h^2$ and Ω_m rather than by calculating the full parameter degeneracies, and we do not use information encoded in the growth of structure.

In Sec.4 we forecast an error $\sigma(w) = 0.026$ for an HI survey with the full SKA with $\beta FOV = 10 \text{ deg}^2$. The error determination in Table 2 is ≈ 4 times smaller. We suggest that approximately half of this improved performance is the result of utilizing the growth factor measurements, and the remainder is the result of using the shape of the power spectrum to measure the values of Ω_m and h more accurately hence sharpening our capacity to utilize the BAO distance information.

6 REMARKS ON SYSTEMATIC ERRORS IN FUTURE RADIO SURVEYS

The forecasts in this paper assume that the HI galaxy clustering measurements are not compromised by systematic errors from spurious sources or artifacts in the data. We present results for 10- σ and 5- σ source catalogues; however, there is a wealth of extra information contained in the lower-sigma peaks in our derived radio images, and our analysis is conservative. In principle it might be possible to analyze the raw intensity data cube without the intermediate step of extracting a catalogue and thereby greatly enhance the maximum redshift and number density of our HI galaxy survey (Chang et al. 2008).

A concern with this approach is our ability to quantify accurately the power spectrum of the noise. Given the dynamic range limitations of radio interferometry, the noise will be highly variable across the sky and depend on a host of subtle calibration issues; it is certainly likely to be enhanced in the vicinity of bright radio continuum sources imprinting characteristic scales in the measurement. The imprint of this variation will require very careful modelling. It is also possible that, in contrast to CMB observations, the noise in the

HI data cube may be non-Gaussian. A detailed investigation of these issues is beyond the scope of this paper.

Another source of systematic error in the galaxy power spectrum is the uncertainty in the galaxy bias factor. This can be investigated by measuring the clustering properties of galaxy sub-samples (split for example by HI mass) across which the imprint of cosmological parameters should be identical. This programme can be carried out effectively for HI surveys owing to the large number density of sources. This is illustrated by Fig.18 – the solid lines show the value of the quantity nP for different models, assuming a 1-yr SKA survey with $\beta FOV \sim 10$, where n is the galaxy number density and P is the power spectrum amplitude. The product $nP > 10$ over a large redshift range, implying that we can measure a power spectrum without serious shot noise error for more than ~ 10 subsets of galaxies. An aggressive (few σ) detection threshold may require more complicated treatments of galaxy bias. Low-threshold catalogues suffer heavily from Eddington bias effects that (considering for simplicity one fixed redshift) will yield a spuriously wide range of intrinsic HI mass (and hence galaxy bias) at the fixed detection HI line detection threshold.

Because this survey is ‘over-sampled’ at low redshifts it is possible to reduce significantly the performance of the telescope without compromising much of the cosmological science. In Fig.18 we consider the case where the sensitivity decreases with the square of the frequency above 800 MHz; the result is the dashed line and this could yield important design considerations: for example a quadratic drop-off in the sensitivity of aperture arrays arises naturally if critical sampling of the wavefront (having antenna elements spaced at least every half wavelength) becomes relaxed below a wavelength, say that corresponding to 800 GHz, meaning that at these higher frequencies the array becomes sparse rather than close packed (Braun & van Capellen 2006). Gaining a clearer idea of the frequency ranges where noise can be compromised depends on a better measurement of the HI mass function at $z \sim 1$, emphasizing the importance of the stacking experiments mentioned in Sec.2.

In our baseline model the full SKA can survey the $z < 2$ Universe on the timescale of a year, based on technologies such as a phased array or dishes with focal-plane phased arrays in order to achieve the required fields of view. At lower frequencies, sparsely-sampled dipoles may be the technology of choice. In this case the scaling of field-of-view with frequency can be set to the user requirements provided that the computing power is available to process the required number of beams. Our assumed $(1+z)^2$ scaling of the FOV is just one choice, that needs to be optimized with detailed simulations. At the lowest frequencies it may be desirable to have the physical collecting area rising as a sharp function of wavelength to ensure a mapping speed that is constant in redshift. For a sparse array this is naturally achieved via the λ^2 variation in the collecting area of antennas. However it may still be necessary to build physically more antennas in this frequency range, or to use the processing system to shape how the FOV varies with frequency, and hence redshift, by, for example, forming more beams at the lower frequencies to yield greater instantaneous sky coverage. This is subject to the fundamental limitation of the finite sky area observable at moderate zenith angle from an aperture array station.

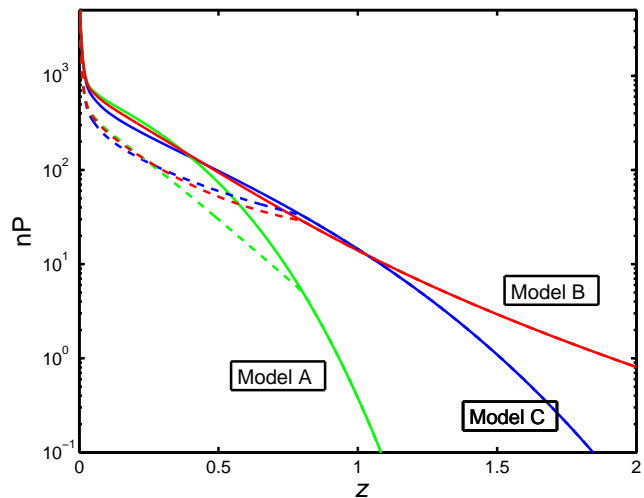


Figure 18. The solid lines display the variation of the value of nP with redshift for the 3 different HI evolution models. For all models the value of nP remains above 1 for $z < 1$, implying that we can measure the galaxy power spectrum for many sub-samples and hence constrain the systematic effects of galaxy bias. The dashed lines illustrate the degradation which occurs when the telescope sensitivity worsens as the frequency squared in the high frequency range, i.e. at low redshift.

7 CONCLUSIONS

We have forecast the cosmological parameter measurements that could result from a combination of future HI-emission galaxy surveys with the SKA and CMB (*Planck*) data. The main degeneracies currently present in cosmological data would be broken by such new surveys. Current parameters would be measured to below the 1% level and other parameters such as neutrino masses will be accessible.

We find that an HI survey with a telescope possessing $f = 0.15$ of the SKA sensitivity, together with a future CMB experiment, will be able to determine the dark energy equation of state with an accuracy close to one per cent. We have examined the origin of this information and found that the robust signature of ‘geometry’ (the projection of the BAOs) is producing significant power. The remaining information originates from measurements of the growth of cosmic structure that can be inferred by looking at redshift-space distortions at large scales and thereby breaking the degeneracy with galaxy bias.

We caution that the evolutionary model considered here adopts a slightly stronger evolution in the cosmic mass density of HI (see Fig. 2) than is inferred from the most recent studies of HI absorption (Pontzen & Pettini 2008), so the observing times required may be underestimated by a small factor (assuming most of the number counts are coming from the exponential tail of the mass function near the break, which should be the case in the high redshift region; in order to have ~ 1.5 times more sources, one would need to detect sources ~ 1.7 times the mass, which would require ~ 2.8 the exposure time roughly). We emphasise the importance of stacking experiments in Sec.2.

A survey with the full SKA would be able to produce a measurement of the dark energy parameter with an ac-

curacy close to half a per cent. In this case the addition of the CMB data does not produce such a substantial increase in performance. However, the SKA and CMB data remain complementary in the sense that the galaxy survey data is better able to measure the height of the power spectrum (hence σ_8) and the CMB data is most powerful for determining the spectral index of scalar fluctuations (n_s).

We conclude that a radio telescope with a sensitivity between $f = 0.15$ and $f = 1$ of the SKA would be a cosmological tool capable of transformational science, particularly in the field of dark energy.

ACKNOWLEDGMENTS

We thank Kathryn Nicklin and Danail Obreschkow for practical help with the work of this paper and for useful discussions. FBA acknowledges support from the Leverhulme Foundation via an Early Careers Fellowship. This work has been undertaken as part of the Square Kilometre Array Design Study (SKADS) financed by the European Commission.

REFERENCES

- Abdalla F. B., Rawlings S., 2005, *MNRAS*, 360, 27
 Abdalla F. B., Rawlings S., 2007, *MNRAS*, 381, 1313
 Basilakos S., Plionis M., Kovač K., Voglis N., 2007, *MNRAS*, 378, 301
 Blake C., Glazebrook K., 2003, *ApJ*, 594, 665
 Blake C., Parkinson D., Bassett B., Glazebrook K., Kunz M., Nichol R. C., 2006, *MNRAS*, 365, 255
 Blake C. A., Abdalla F. B., Bridle S. L., Rawlings S., 2004, *New Astronomy Review*, 48, 1063
 Boughn S. P., Crittenden R. G., 2005, *New Astronomy Review*, 49, 75
 Braun R., van Capellen W., 2006
 Cabré A., Gaztañaga E., Manera M., Fosalba P., Castander F., 2006, *mnras*, 372, L23
 Chang T.-C., Pen U.-L., Peterson J. B., McDonald P., 2008, *Physical Review Letters*, 100, 091303
 Choudhury T. R., Padmanabhan T., 2002, *ApJ*, 574, 59
 Cimatti A., the SPACE collaboration 2008, *Experimental Astronomy*, pp 37–+
 Cole S., Sanchez A. G., Wilkins S., 2006, *ArXiv Astrophysics e-prints*
 Cruz M. J., Jarvis M. J., Rawlings S., Blundell K. M., 2007, *mnras*, 375, 1349
 Dalton G. B., Lewis I. J., Bonfield D. G., Holmes A. R., Brooks C. B., Lee H., Tosh I. A. J., Froud T. R., Patel M., Dipper N. A., Blackburn C., 2006, in *Ground-based and Airborne Instrumentation for Astronomy*. Edited by McLean, Ian S.; Iye, Masanori. *Proceedings of the SPIE*, Volume 6269, pp. 62694A (2006). Vol. 6269 of Presented at the Society of Photo-Optical Instrumentation Engineers (SPIE) Conference, The UK FMOS spectrograph
 Dunkley J., Komatsu E., Nolte M. R., Spergel D. N., Larson D., Hinshaw G., Page L., Bennett C. L., Gold B., Jarosik N., Weiland J. L., Halpern M., Hill R. S., Kogut A., Limon M., Meyer S. S., Tucker G. S., Wollack E., Wright E. L., 2008, *ArXiv e-prints*, 803
 Eisenstein D. J., Hu W., 1998, *ApJ*, 496, 605
 Eisenstein et al. 2005, *ApJ*, 633, 560
 Ellison S. L., Yan L., Hook I. M., Pettini M., Wall J. V., Shaver P., 2001, 379, 393
 Freedman W. L., Madore B. F., Gibson B. K., Ferrarese L., Kelson D. D., Sakai S., Mould J. R., Kennicutt R. C., Ford H. C., Graham J. A., Huchra J. P., Hughes S. M. G., Illingworth G. D., Macri L. M., Stetson P. B., 2001, *ApJ*, 553, 47
 Giannantonio T., Crittenden R. G., Nichol R. C., Scranton R., Richards G. T., Myers A. D., Brunner R. J., Gray A. G., Connolly A. J., Schneider D. P., 2006, *prd*, 74, 063520
 Glazebrook K., Blake C., 2005, *ApJ*, 631, 1
 Glazebrook K., Blake C., Couch W., Forbes D., Drinkwater M., Jurek R., Pimblet K., Madore B., Martin C., Small T., Forster K., Colless M., Sharp R., Croom S., Woods D., Pracy M., Gilbank D., Yee H., Gladders M., 2007, in *Metcalf N., Shanks T., eds, Cosmic Frontiers Vol. 379 of Astronomical Society of the Pacific Conference Series, The WiggleZ Project: AAOmega and Dark Energy*. pp 72–+
 Guzzo et al. 2008, *Nat*, 451, 541
 Hill G. J., Gebhardt K., Komatsu E., Drory N., MacQueen P. J., Adams J., Blanc G. A., Koehler R., Rafal M., Roth M. M., Kelz A., Gronwall C., Ciardullo R., Schneider D. P., 2008, *ArXiv e-prints*, 806
 Hu W., Haiman Z., 2003, *Phys. Rev. D*, 68, 063004
 Ishibashi A., Wald R. M., 2006, *Classical and Quantum Gravity*, 23, 235
 Komatsu E., Dunkley J., Nolte M. R., Bennett C. L., Gold B., Hinshaw G., Jarosik N., Larson D., Limon M., Page L., Spergel D. N., Halpern M., Hill R. S., Kogut A., Meyer S. S., Tucker G. S., Weiland J. L., Wollack E., Wright E. L., 2008, *ArXiv e-prints*, 803
 Lahav et al. 2002, *MNRAS*, 333, 961
 Mena O., Santiago J., Weller J., 2006, *Physical Review Letters*, 96, 041103
 Péroux C., Irwin M. J., McMahon R. G., Storrie-Lombardi L. J., 2001, *Astrophysics and Space Science Supplement*, 277, 551
 Percival W. J., Nichol R. C., Eisenstein D. J., Frieman J. A., Fukugita M., Loveday J., Pope A. C., Schneider D. P., Szalay A. S., Tegmark M., Vogeley M. S., Weinberg D. H., Zehavi I., Bahcall N. A., Brinkmann J., Connolly A. J., Meiksin A., 2007, *ApJ*, 657, 645
 Percival W. J., Nichol R. C., Eisenstein D. J., Weinberg D. H., Fukugita M., Pope A. C., Schneider D. P., Szalay A. S., Vogeley M. S., Zehavi I., Bahcall N. A., Brinkmann J., Connolly A. J., Loveday J., Meiksin A., 2007, *ApJ*, 657, 51
 Percival W. J., White M., 2008, *ArXiv e-prints*, 808
 Péroux C., Dessauges-Zavadsky M., D’Odorico S., Sun Kim T., McMahon R. G., 2005, *MNRAS*, 363, 479
 Pontzen A., Pettini M., 2008, *ArXiv e-prints*
 Prochaska J. X., Herbert-Fort S., Wolfe A. M., 2005, *ApJ*, 635, 123
 Räsänen S., 2004, *Journal of Cosmology and Astro-Particle Physics*, 2, 3
 Rassat A., Land K., Lahav O., Abdalla F. B., 2006, *ArXiv Astrophysics e-prints*
 Rawlings S., Abdalla F. B., Bridle S. L., Blake C. A., Baugh C. M., Greenhill L. J., van der Hulst J. M., 2004, *New*

- Astronomy Review, 48, 1013
- Refregier A., the DUNE collaboration 2008, ArXiv e-prints
- Riess et al. 2006, ArXiv Astrophysics e-prints
- Seo H.-J., Eisenstein D. J., 2003, ApJ, 598, 720
- Seo H.-J., Eisenstein D. J., 2007, ApJ, 665, 14
- Simpson F., Bridle S., 2006, prd, 73, 083001
- Skordis C., Mota D. F., Ferreira P. G., Boehm C., 2006, Physical Review Letters, 96, 011301
- Spergel et al. 2007, apjs, 170, 377
- Taylor A. R., Braun R., eds, 1999, Science with the Square Kilometer Array : a next generation world radio observatory
- Thompson A. R., Moran J. M., Swenson Jr. G. W., 2001, Interferometry and Synthesis in Radio Astronomy, 2nd Edition. Interferometry and synthesis in radio astronomy by A. Richard Thompson, James M. Moran, and George W. Swenson, Jr. 2nd ed. New York : Wiley, c2001.xxiii, 692 p. : ill. ; 25 cm. "A Wiley-Interscience publication." Includes bibliographical references and indexes. ISBN : 0471254924
- Verde et al. 2002, MNRAS, 335, 432
- Verheijen M. A. W., van Gorkom J. H., Szomoru A., Dwarakanath K. S., Poggianti B. M., Schiminovich D., 2007, ArXiv e-prints, 708
- Zhang P., Pen U.-L., 2006, MNRAS, 367, 169
- Zwaan M. A., Meyer M. J., Staveley-Smith L., Webster R. L., 2005, MNRAS, 359, L30
- Zwaan M. A., van Dokkum P. G., Verheijen M. A. W., 2001, Science, 293, 1800
- Zwaan et al. 2003, AJ, 125, 2842